JOURNAL OF GEOPHYSICAL RESEARCH, VOL. 113, C11013, doi:10.1029/2008JC004756, 2008

Estimates of sea surface height and near-surface alongshore coastal currents from combinations of altimeters and tide gauges

M. Saraceno,[1,2] P. T. Strub,[1] and P. M. Kosro[1]

Received 31 January 2008; revised 8 August 2008; accepted 25 August 2008; published 15 November 2008.

[1] Present methods used to retrieve altimeter data do not provide reliable estimates of sea surface height (SSH) in the nearshore region, resulting in a measurement gap of 25–50 km next to the coast. In the present work, gridded SSH fields produced by Archiving, Validation, and Interpretation of Satellite Oceanographic data (AVISO) in the offshore region are combined with coastal tide gauge time series of SSH to improve estimation in that gap along the west coast of the United States in the northern California Current System between 40° and 45°N and 123.8° and 126°W. To assess the increase in skill provided by this procedure, the geostrophic alongshore currents, calculated from the new SSH fields in the gap region, are compared to three in situ, nearshore current measurements, resulting in correlation coefficients of 0.73–0.83 and standard deviations of the differences of 11.6–12.6 cm/s, substantially improved from the AVISO-only results. When the Ekman current components are estimated and added to the geostrophic currents, comparisons to the 10 m deep acoustic Doppler current profiler velocities are only slightly improved. The Ekman components make a more significant contribution when compared to HF radar surface current measurements, providing correlations of 0.94 and standard deviations of the differences of 6.4–9.5 cm/s. These results represent a dramatic improvement in the quality of the SSH fields and estimated alongshore currents when additional, realistic SSH data from the coastal region are added. Here we use coastal tide gauges to provide the additional SSH data but also discuss more general approaches for altimeter SSH retrievals in coastal regions where tide gauge data are not available.

Citation: Saraceno, M., P. T. Strub, and P. M. Kosro (2008), Estimates of sea surface height and near-surface alongshore coastal currents from combinations of altimeters and tide gauges, *J. Geophys. Res.*, *113*, C11013, doi:10.1029/2008JC004756.

1. Introduction

[2] Satellite altimetry provides a unique opportunity to understand the dynamics of the sea, with sea surface height (SSH) data extending over the past 15 or more years. The usefulness of the altimeter measurements for large-scale studies is well established, as demonstrated by studies of the large-scale California Current on seasonal and interannual timescales [*Kelly et al.*, 1998; *Strub and James*, 2000, 2002a, 2002b]. However, coastal processes are more difficult to resolve with altimeter data, because of two types of problems. First, and most importantly, intrinsic difficulties affect the corrections applied to the altimeter data near the coast (e.g., the wet tropospheric component, high-frequency oceanographic signals, tidal corrections, etc.). Thus, data are usually flagged as unreliable within some distance of the coast. Second, the interpolation of along-track data collected by just one or two satellites provides only marginal resolution of mesoscale and smaller-scale structure in ocean circulation [*Le Traon and Dibarboure*, 2002; *Leeuwenburgh and Stammer*, 2002; *Chelton and Schlax*, 2003], which is dominant in the coastal region.

[3] Several approaches are available to address the problems described above. *Pascual et al.* [2006, 2007] show that increasing the number of satellites used to produce gridded maps of sea surface height to four greatly increases the accuracy of estimates of the mesoscale surface circulation. *Volkov et al.* [2007] show that improvements in tidal and high-frequency models used to produce the data distributed by the Archiving, Validation, and Interpretation of Satellite Oceanographic data (AVISO) project also improve the quality of the altimeter SSH fields over wide continental shelves. Other efforts to correct the altimeter signal near the coast include recomputing the wet tropospheric correction [*Manzella et al.*, 1997; *Vignudelli et al.*, 2005; *Madsen et al.*, 2007; *Desportes et al.*, 2007], the use of customized tidal modeling [*Vignudelli et al.*, 2000; *Volkov et al.*, 2007], the use of higher-rate data [*Lillibridge*, 2005], and/or retracking [*Deng and Featherstone*, 2006].

[4] In the present work we address the first set of problems described above by first estimating the distance from the coast within which the original along-track altim-

[1]College of Oceanic and Atmospheric Sciences, Oregon State University, Corvallis, Oregon, USA.
[2]Currently at Centro de Investigaciones del Mar y la Atmosfera, Ciudad Universitaria, Buenos Aires, Argentina.

0148-0227/08/2008JC004756$09.00

eter data are usually (>75% of the time) flagged as unreliable. Because of the lack of valid data, gridded AVISO altimeter fields in this coastal "gap" region are mostly the result of the extrapolation of nearby offshore data. However, as we shall show, this procedure is often unreliable. After eliminating the AVISO data in this gap, we produce new SSH fields by interpolating between the tide gauge SSH data set along the coast and the gridded SSH data set produced by AVISO in the offshore region. To assess the improvement resulting from this simple approach, alongshore geostrophic currents, estimated from the new SSH fields, are then compared to in situ acoustic Doppler current profiler (ADCP) currents and surface current measurements from CODAR SeaSonde HF mapping systems ("HF currents") within the gap and the statistics of the comparisons are presented.

[5] The domain considered in this work is the northern California Current System (CCS) between 40° and 45°N and 123.8° and 126°W. In most of this region, the continental shelf is relatively narrow and deep, reducing the effects of tidal model errors in the altimeter data set. This portion of the coastal ocean off Oregon has been the focus of a number of in situ process studies, beginning with the Wisp and Coastal Upwelling Experiments (CUE-I and CUE-II) in the early 1970s, continuing through the GLOBEC (Global Ocean Ecosystem Experiment) and COAST (Coastal Ocean Advances in Shelf Transport) projects during 1997–2003. The early studies resulted in two-dimensional (onshore-offshore) conceptual models of upwelling systems [*Kundu et al.*, 1975; *Kundu and Allen*, 1976; *Huyer et al.*, 1978, 1979]. The in situ current measurements, surveys and satellite data starting in 1997 revealed greater three-dimensional complexity in the mesoscale circulation fields [*Barth et al.*, 2000, 2005a, 2005b; *Kosro*, 2005]. The results of studies through the early 1990s are included in reviews of the CCS physical oceanography by [*Hickey*, 1979, 1998]. *Mackas et al.* [2006] include the later studies and extend the scope of the review to include biological responses to the physical forcing, upwelling and mesoscale circulation patterns.

[6] In the northern CCS, wind stress, coastal SSH and strong coastal currents reverse seasonally [*Hickey*, 1979; *Strub et al.*, 1987; *Hickey*, 1998; *Strub and James*, 2000; *Huyer et al.*, 2007]. In spring and summer, persistent equatorward winds (associated with the North Pacific High) produce upwelling, low sea levels next to the coast and an equatorward flowing jet that is found over or offshore of the shelf. In fall and winter, poleward winds (associated with synoptic storms) produce downwelling, high sea levels next to the coast and a poleward coastal jet, sometimes called the Davidson Current. In addition to forcing by the local or regional wind stress, buoyancy forcing by freshwater discharge at the coast influences the coastal circulation in some locations, especially near the Columbia River Plume [*Hickey*, 1998; *Huyer et al.*, 2005]. Winds located farther to the south (off northern California) are also important, communicating their influence to the coastal ocean off central Oregon through the passage of poleward propagating coastal trapped waves (CTW) [*Allen*, 1975; *Smith*, 1978; *Brink*, 1991; *Hickey et al.*, 2006].

[7] Tide gauges are commonly used to calibrate and validate altimeter data [*Leuliette et al.*, 2004], making them a natural choice to extend altimeter SSH data to the coast. In an early use of combinations of tide gauge and altimeter SSH data *Strub and James* [1997] demonstrated that the inclusion of tide gauge data allowed the SSH fields to show the early development of an equatorward jet over the narrow shelf off central California in spring. The jet became visible in the altimeter-only fields when it moved farther offshore. Off Oregon, the jet stays over the shelf and closer to the coast for much of the spring and early summer [*Kosro*, 2005], making it less visible to the altimeter-only SSH fields.

[8] In the region studied here, five tide gauges are distributed approximately evenly in latitude, providing long-term SSH measurements. In addition, three in situ moorings with ADCPs [*Kosro*, 2003; *Geier et al.*, 2006] and an array of HF surface current radars along the coast [*Kosro*, 2006] provide long-term current measurements for part of the altimeter period that can be used to validate the increased skill in geostrophic alongshore velocities estimated from the new SSH fields in the coastal "gap." The presence of strongly varying seasonal and synoptic currents, tide gauges, in situ current measurements and fairly simple coastal geometry makes this an ideal location to test the ability of combinations of altimeter and tide gauge data to resolve the alongshore coastal circulation.

[9] This article is organized as follows: In section 2 we present the satellite altimeter and tide gauge data, as well as the in situ current meters and high-frequency surface current maps that are used to validate the results. In section 3, the methodology used to interpolate the data is explained and the new gridded maps of SSH are compared to the maps produced by AVISO. Geostrophic velocities derived from the new SSH fields are compared to three time series of in situ current measurements and to the HF surface current maps in section 4, before and after adding Ekman components. A discussion of the results, their limitations and possible future extensions concludes the article in section 5.

2. Data

2.1. Satellite Altimetry

[10] Two type of satellite altimeter data are used in the present work: along-track and gridded, both downloaded from the AVISO ftp site (data are available at ftp://ftp.cls.fr). We downloaded the along-track delayed time Geophysical Data Record (GDR) and the delayed time, updated version of the AVISO sea level anomaly weekly maps gridded at 1/4° in rectangular projection. The gridding technique for combining multisatellite data is described by *Le Traon et al.* [2003]. AVISO gridded data are widely used to study the large-scale and mesoscale currents, as well as to evaluate model SSH and surface current fields (data are available at http://sealevel.jpl.nasa.gov). All data were corrected at AVISO, using standard techniques for instrumental noise, orbit error, atmospheric attenuation (wet and dry tropospheric and ionospheric effects), sea state bias, etc. A global adjustment using the Topex/Poseidon (T/P) orbit as a reference was performed to remove biases for all satellites [*Le Traon and Ogor*, 1998]. Since 2005, all data have been retreated with a new tidal model (GOT2000) and a correction for the aliased high-frequency signals using a hydrodynamic model (MOG2D-G) [*Carrère and Lyard*, 2003]. The benefits in shallow waters of

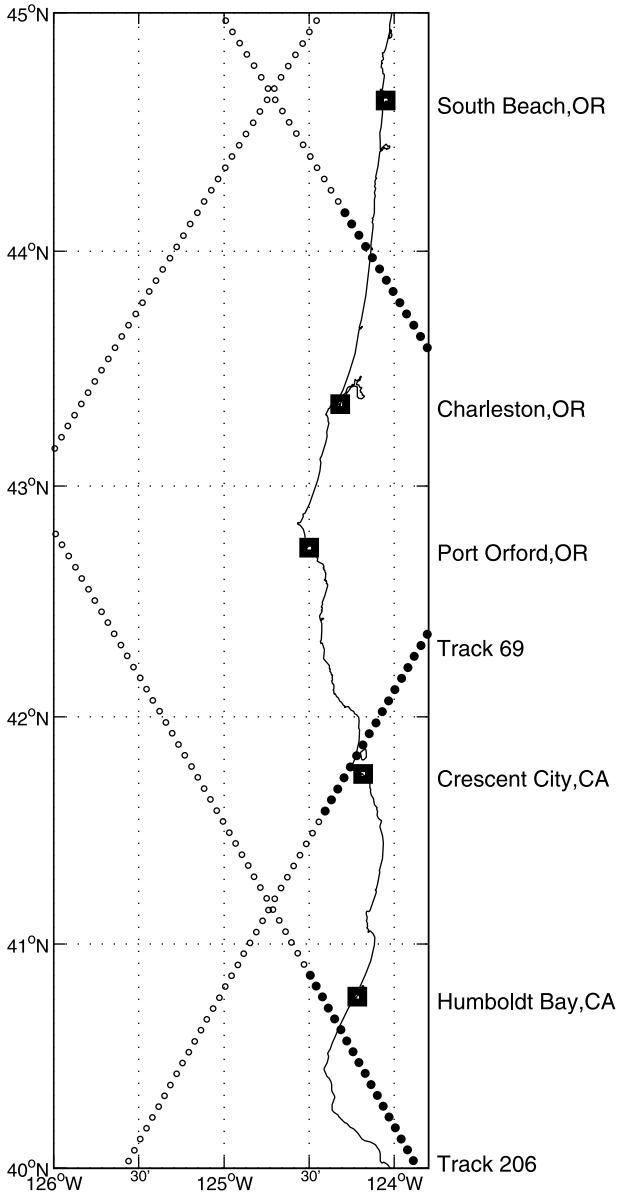

Figure 1. Along-track positions of Topex and Jason data. Empty (filled) circles indicate positions where more (less) than 75% of the data are present during the period January 1993 to December 2005. The positions of the tide gauges are indicated with filled squares.

those corrections compared to previous versions of the data are discussed by *Volkov et al.* [2007]. Despite those corrections, along-track data show an important percentage of missing data as they approach the coast as quantified in section 3.2. However, the gridded AVISO fields do not have a consistent gap near the coast, because of the extrapolation of the data to the coast (and over the coast, in some locations).

2.2. Tide Gauge Data

[11] Research quality hourly tide gauge (TG) data were downloaded from the University of Hawaii Sea Level Center (data are available at http://ilikai.soest.hawaii.edu/uhslc) for the same time period considered for the SSH: January 1993 to December 2005. Data were retrieved from five stations distributed between 40°N and 45°N (Figure 1 and Table 1), with minimum and maximum distances between TGs of 70 km and 144 km. There are gaps in the records at Port Orford (Oregon) and Crescent City (California); at the other three TGs, water level measurements were uninterrupted for the period January 1993 to December 2005. These tide gauge records are from newer instruments and do not contain the type of errors described by *Lentz* [1993] and *Harms and Winant* [1994].

2.3. Independent Current Measurements

[12] In order to quantify the accuracy of the SSH produced by merging TG and satellite data in the nearshore region, we correlated the geostrophic velocities derived from the new SSH fields with three in situ time series of velocities estimated from upward looking acoustic Doppler current profilers (ADCP) (see locations in Table 1) and HF surface current maps. The moorings are part of the U.S. Global Ocean Ecosystem Dynamics (GLOBEC) program [*Kosro*, 2003; *Geier et al.*, 2006]. HF surface current maps are produced by the Ocean Currents Mapping Lab, Oregon State University [*Kosro*, 2006] (data are available at http://bragg.coas.oregonstate.edu/) using an array of four long-range SeaSonde high-frequency surface current mappers distributed along the Oregon coast, inside the region considered. The methodology for these systems has been described [*Barrick et al.*, 1977; *Lipa and Barrick*, 1983]. We used 1 year (2002) of low-pass filtered (46-h half power) gridded maps of HF surface currents.

2.4. Wind Data

[13] We used wind stress data to compute Ekman currents at the locations corresponding to the position of the moor-

Table 1. Location Name, Type of Instrument, Nearest Location at the Coast, Position, and Beginning and Ending Dates of the Time Series[a]

Name of Location	Instrument	Latitude (°N)	Longitude (°W)	Dates		Bin/Total Depth (m)
				Start	End	
Newport, Oregon	ADCP	44.65	124.31	9 Aug 1997	31 Dec 2005	11/81
Coos Bay, Oregon	ADCP	43.16	124.57	22 Apr 2000	6 Sep 2004	10/100
Rogue River, Oregon	ADCP	42.44	124.57	9 Nov 2000	8 Sep 2004	10/69
Crescent City, California	TG	41.7	124.18	1 Jan 1993	31 Dec 2005	
Port Orford, Oregon	TG	42.74	124.62	1 Jan 1993	31 Dec 2005	
Charleston, California	TG	43.34	124.32	1 Jan 1993	31 Dec 2005	
South Beach, Oregon	TG	44.63	124.04	1 Jan 1993	31 Dec 2005	
Humboldt Bay, California	TG	40.77	124.22	1 Jan 1993	31 Dec 2005	

[a]Depths of the velocity bin used and the total local depths are also indicated for the ADCPs. ADCP, acoustic Doppler current profiler; TG, tide gauge.

Table 2. Correlation Between the Meridional Wind Stress Components as Estimated by QuikSCAT and Buoys[a]

		QuikSCAT Versus Buoys	
Name of Location	Latitude (°N)	Correlation (95% CL)	SD (Difference) (Pa)
Newport, Oregon	44.65	0.72 (0.16)	0.09
Coos Bay, Oregon	43.16	0.75 (0.22)	0.12
Rogue River, Oregon	42.44	0.79 (0.23)	0.14

[a]The standard deviations (SD) of the differences between time series are also shown. CL, Confidence Level.

ings with the ADCP. Wind stress is computed from wind speed, which in the ocean is measured by in situ buoys or by the satellite scatterometer QuikSCAT. To decide which source of data to use, we compared both. Wind data from buoys were downloaded from the NOAA National Data Buoy Center website (www.ndbc.noaa.gov). The mooring located at Newport (South Beach) is very close (15.5 Km) to buoy 46050, which provides wind speed measurements. Unfortunately, this is not the case for the other two moorings: the nearest buoy (46015) provides measurements only since 21 July 2002, with a gap of nine months between October 2003 and July 2004. On the other hand, QuikSCAT data provide complete coverage of the surface of the ocean since 20 July 1999 to the present. We downloaded from the Ifremer web site (data are available at www.ifremer.fr/cersat/) a gridded version of the QuikSCAT wind stress at daily temporal resolution and $0.5^\circ \times 0.5^\circ$ spatial resolution. Three time series were extracted at the locations nearest to the moorings. The meridional component of the wind stress (which is the component that explains the highest percentage of variance) as measured by QuikSCAT and by the buoys are very similar (Table 2). Thus, we used the wind stress estimated by the more complete QuikSCAT time series to compute the Ekman currents.

3. Methods

3.1. Preliminaries

3.1.1. Correlations

[14] All the correlation coefficients cited are significant at 95% Confidence Level (CL), unless otherwise indicated. The significance levels of the scalar squared correlations are estimated from the χ^2 distribution on the basis of the number of independent observations (N*) estimated using the long lag method, following *Davis* [1976].

3.1.2. TG Calibration

[15] To suppress any tide-related signal, all TG data were low-pass filtered with a 40-h (half power) Loess filter [*Cleveland and Devlin*, 1988]. Then, the inverse barometer correction was applied using the 6-h reanalysis of Sea Level Pressure produced by the National Centers for Environmental Prediction (NCEP).

3.1.3. Low-Pass Filtering and SSH Calibration

[16] The Nyquist frequency of the T/P and Jason data is 1/20 cycles per day. Thus a 20-day half-power Loess filter was applied to the inverted barometer corrected TG time series. Current meter time series have also been low-pass filtered with the same 20-day low-pass Loess filter.

[17] We estimate SSH anomalies by subtracting the time average of the total record length at each point in the altimeter SSH gridded maps and at the five TGs. This keeps all time-varying gradients of heights, the strongest of which are associated with seasonal changes in alongshore jets, mesoscale meanders or eddies. Considering the relative small region used in the present work and that we are interested in highlighting mesoscale structures, we prefer not to add uncertainties by adding a nonprecise mean dynamic height (from climatology) to restore the largest-scale features. Mean dynamic heights in the region present a slight slope in the onshore-offshore direction, with lower values next to the coast [*Strub and James*, 2002a], consistent with weak (2–3 cm/s) equatorward flow. The analysis of temporal variability is not affected by the exclusion of this slope.

3.2. Estimation of the Gap

[18] Six satellite missions have collected SSH data during our period of interest: Topex/Poseidon (T/P), ERS-1/2, Jason 1, Geosat Follow-On (GFO) and Envisat. Among those, T/P and Jason 1 shared the same tracks producing a long record (23 September 1992 to present) at the highest frequency (orbital repeat period is 9.916 days). Two of the T/P and Jason tracks that cover the region considered here pass very close to two of the tide gauges (Figure 1): the shortest distance between track 206 and the tide gauge at Humboldt Bay is 15.8 km; between track 69 and the tide gauge at Crescent City, it is 6.8 km. These two tracks are used to estimate the correlations between TGs and along-track SSH time series (Figure 2), which determine the distance from the coast at which the satellite altimeter become routinely usable. For this purpose, a single time series from January 1993 to December 2005 is constructed from the T/P and Jason time series at each spatial location of the along-track data. T/P flew between 23 September 1992 and 25 August 2002 and Jason 1 has been flying since 15 January 2000. Thus, before merging the data from the different missions it is necessary to eliminate any differences (biases) between T/P and Jason 1 SSH measurements. In order to do so, the following occurred:

[19] 1. We added to the T/P time series the time mean of the difference between it and the Jason 1 time series. The difference is estimated during the period when both satellites flew in the same orbits (15 January 2002 to 25 August 2002).

[20] 2. The temporal mean (estimated between January 1993 and December 2005) at each location is also removed.

[21] More than 75% of the data available at each along-track position are missing at distances shorter than 37 km from the coast (Figures 1 and 2). This is due to intrinsic difficulties in the corrections of the altimeter data (e.g., the wet tropospheric component, high-frequency oceanographic signal, and tidal corrections) as well as issues related to land contamination in the footprint. At distances farther than 37 km from the coast, less than 25% of the data are missing (Figure 1) and the correlation between the TG and the along-track data decreases linearly with distance from the coast (Figure 2). Thus we eliminated all of the gridded data estimated by AVISO that fall within 37 km of the coast.

3.3. Creating a Denser TG Data Set Along the Coast

[22] The five time series of the filtered TGs are very well correlated: among the 10 pairs of possible combinations, the

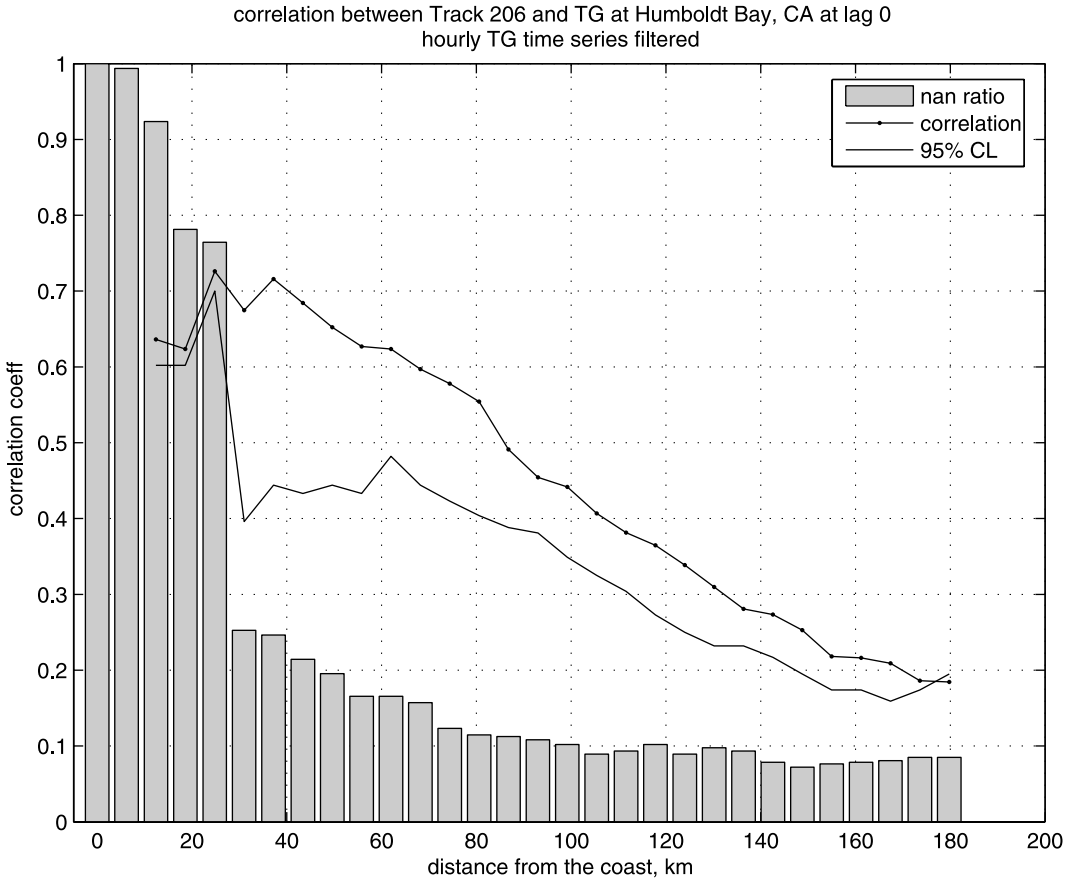

Figure 2. Correlation coefficient (line with dots) and 95% CL (solid line) between time series of sea level anomaly estimated from the TG at Humboldt Bay (California) and as measured by Topex and Jason along track 206, as a function of the distance from the coast. Vertical bars indicate the fraction of satellite data missing at each position along track 206.

minimum correlation is still very high (0.87, between South Beach, Oregon and Humboldt Bay, California, the most widely separated pair) indicating that at this scale, the signal retrieved by the TGs is quite uniform along the coast on timescales of 20 days and longer. This result suggests that in this region it is possible to create a denser spatial array of *virtual* tide gauges, uniformly distributed in latitude with no gaps in time. This is shown in Figure 3 (bottom), where the original TGs have been interpolated into *virtual* TGs evenly distributed along the coast, separated by 0.2° in latitude. The dense TG time series were also subsampled every 7 days to match the exact SSH AVISO gridded dates.

3.4. Covering the Gap: Interpolation of TG With Satellite Data

[23] To cover the gap next to the coast (i.e., the nearshore region indicated in Figures 4 (middle) and 5 (middle), the dense TG SSHs data set is interpolated to the AVISO gridded SSHs in the offshore region (i.e., west of the gap). Our approach here is to use a widely available method that is based on the Delaunay triangulation method [*Delaunay*, 1934]. The Delaunay triangulation technique consists of building a set of triangles by connecting all the data points in such a way that the vertices of the triangles are the data points. The collection of the edge's triangles satisfies an "empty circle" property: for each edge it is possible to find a circle containing the edge's endpoints but not containing any other data points. Figures 4 (middle) and 5 (middle) show the AVISO and TGs data sets (colored points), the regular grid (small black points) and the triangles selected by the Delaunay triangulation (black lines). The value at each grid point in the gap results from the weighted mean of the three data points located at the vertices of the triangle that circumscribes the grid points considered, with weights that are inversely proportional to the distance between the grid points and the data points. This technique is implemented by the "griddata" function in MATLAB, which uses the Quickhull algorithm [*Barber et al.*, 1996]. The interpolated time series produced by the "griddata" function are not significantly different from results obtained by applying an optimal interpolation method [*Marcotte*, 1991] to a limited representative number of fields. An advantage of using optimal interpolation methods is that they provide estimates of the errors. However, for the present application, error estimates are provided by the comparisons to in situ data.

[24] In the next subsection we estimate the geostrophic velocities associated with the new SSH fields. Because the geostrophic velocities are proportional to the slope of the SSH, we applied a running median filter with a window size of 3×3 grid points to the individual SSH fields to avoid any discontinuities in the first derivative of the SSH fields at

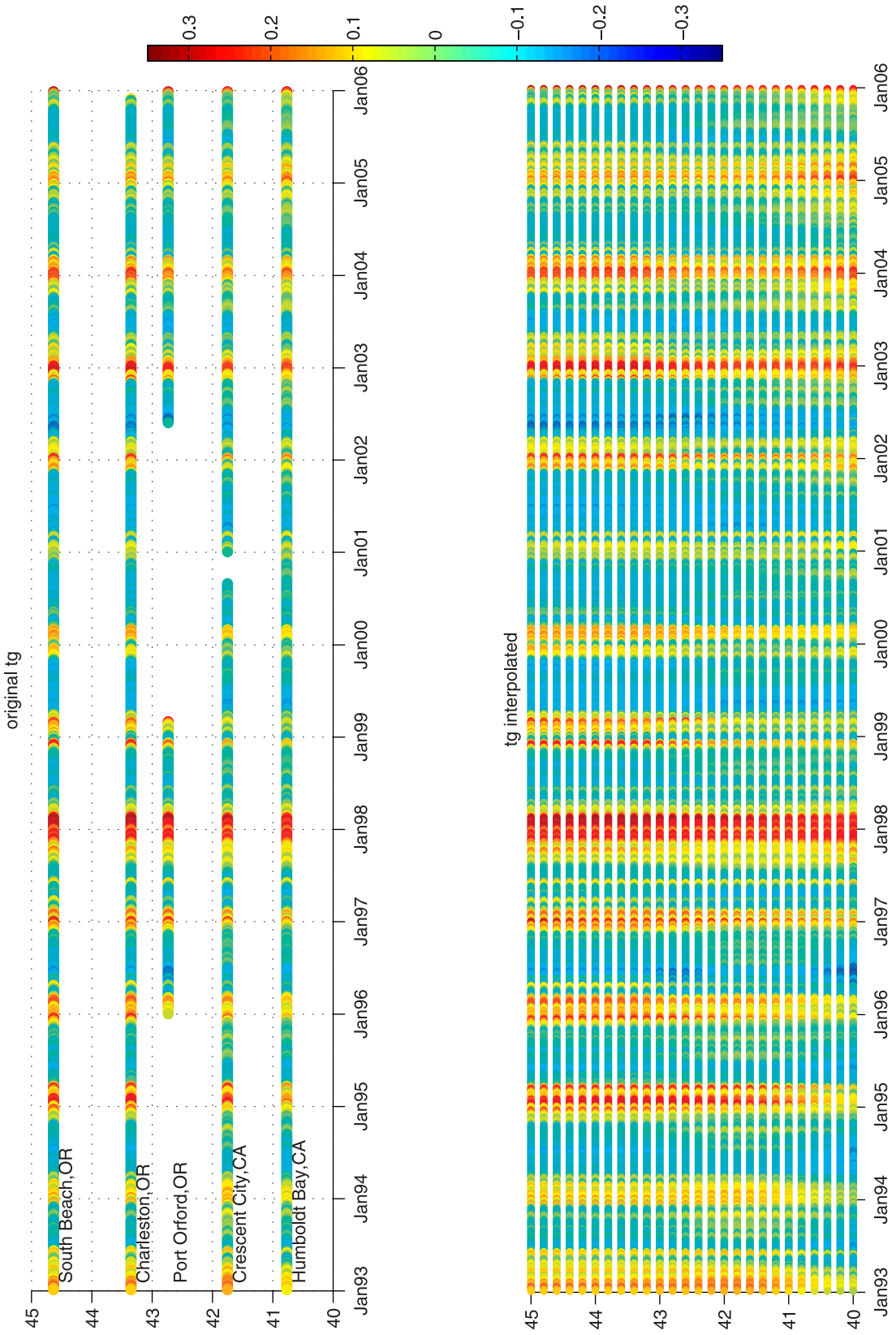

Figure 3. (top) Time series of SSH (m) as measured by the five tide gauges. (bottom) Results of the interpolation of the five TGs' time series to a denser alongshore grid (Figure 4).

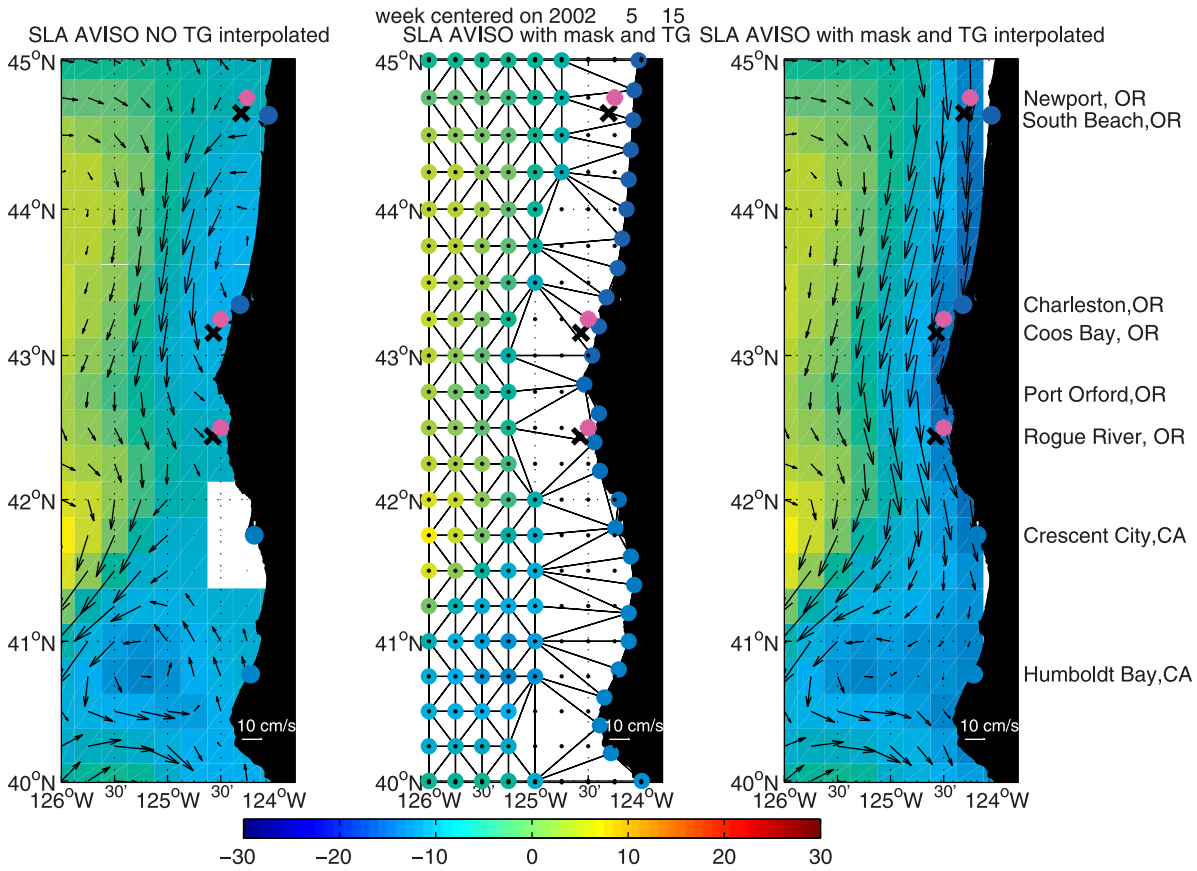

Figure 4. An example of the interpolation of the SSH (cm) measured by TGs with the SSH measured by satellite altimetry, for the week centered on 15 May 2002. (left) Gridded SSH as provided by AVISO. Values measured by the TGs are indicated with color-filled (blue) dots. (middle) SSH from AVISO data that are at a distance greater than 37 km from the coast and the denser array of interpolated TG SSH values along the coast, represented by color-filled dots. Black lines indicate the Delaunay triangles, constructed to interpolate the satellite data with the TG data. Black dots indicate the position of the interpolation grid. (right) The result obtained from the interpolation of the TGs with the satellite data. Vectors on Figure 4 (left) and Figure 4 (right) indicate geostrophic currents estimated from the gridded SSHs. In Figure 4 (left), Figure 4 (middle), and Figure 4 (right), black crosses indicate positions of the ADCPs; magenta-filled points indicate the interpolation grid points for alongshore velocities nearest to the ADCPs.

their boundaries with the AVISO data along the edges of the gap region. Two examples of the result are shown in Figures 4 (right) and 5 (right).

3.5. Geostrophic Currents

[25] We estimate the geostrophic currents for each field that resulted from merging TGs and satellite SSH. The zonal and meridional components of the geostrophic velocity at a given grid point are estimated using centered difference as:

$$u(x,y) = -\left(\frac{g}{f}\right) \cdot \frac{SSH_{x,y+1} - SSH_{x,y-1}}{d(x; y+1, y-1)} \quad (1)$$

$$v(x,y) = \left(\frac{g}{f}\right) \cdot \frac{SSH_{x+1,y} - SSH_{x-1,y}}{d(x+1, x-1; y)}, \quad (2)$$

respectively, where f is the Coriolis parameter, g is the gravitational force and d is the distance between the grid points used in the calculation. In order to estimate values as close as possible to the coast, adjacent SSH values at grid points next to the coast were linearly extrapolated to values that were over the land before using the centered difference formula at the grid point next to the coast. The same equations were used to derive geostrophic velocities from the SSH produced by AVISO.

4. Results

4.1. Geostrophic Result

[26] Figures 4 (right) and 5 (right) show two examples of the results obtained by the interpolation of the TG with the offshore satellite SSH for strong upwelling-favorable (Figure 4) and downwelling-favorable (Figure 5) winds that prevail in the region during summer and winter, respectively [e.g., *Hickey*, 1998, and references therein]. Both SSHs and geostrophic velocities estimated after the inclusion of the TGs show significant differences compared to the AVISO

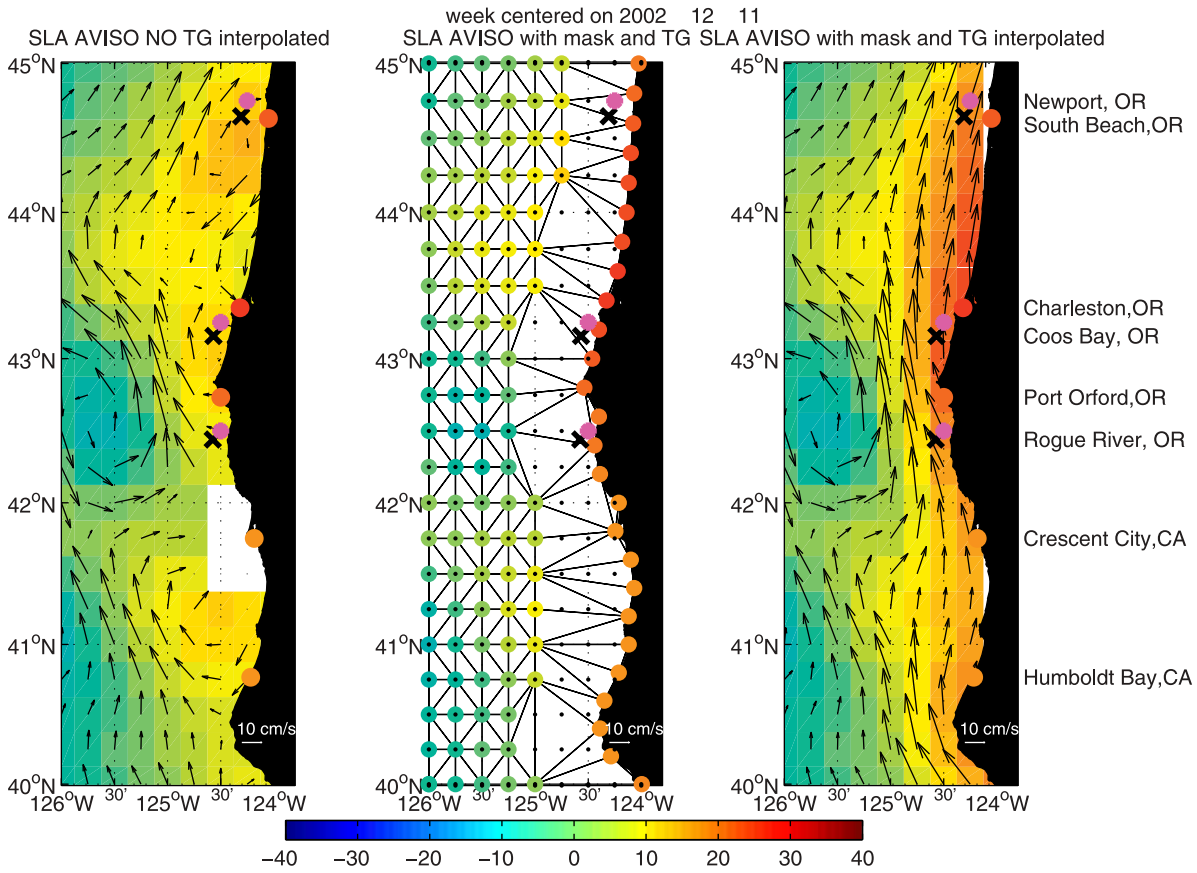

Figure 5. As in Figure 4 but for the week centered on 11 December 2002.

fields in the nearshore region (Figures 4 (left) and 5 (left)). The inclusion of the TGs produces a more continuous, southward (northward) pattern of velocities for the upwelling-favorable (downwelling-favorable) case, compared to the alongshore currents estimated solely from the AVISO data.

[27] To quantify which of these patterns better represent the real currents in the region, we estimate the correlations and standard deviations of the differences between the three ADCP measurements of the currents at 10 m depth and the geostrophic currents at the nearest positions (Table 3 and locations shown in Figures 4 and 5). The time series are shown in Figure 6.

[28] For simplicity, the meridional components of the velocities are used in all of the analyses reported in this paper. The principal axes of variance of the three in situ ADCP time series are within 27° of true north, reflecting the fact that the local currents are well aligned with the contours of the local bathymetry. The correlations and standard deviations summarized in Table 3 have also been estimated after projecting the velocities onto their respective major axes, with no significant change in the results. The correlation at the three sites is higher than 0.74 and the standard deviation of the difference is lower than 12.5 cm/s when the TGs are included. When the geostrophic meridional velocities are estimated from the AVISO SSH data alone, the time series are very weak (Figure 6), the variance of the difference between the time series and the in situ velocities more than doubles, the standard deviation of the difference is increased by at least 5.5 cm/s and all of the correlations

Table 3. Correlations and Standard Deviations of the Differences Between Velocities Estimated From SSH and ADCP Measurements[a]

	Without TG (AVISO Only)		With TG		With TG and Ekman	
Name of Location	Correlation (95% CL)	ST (Difference, in cm/s)	Correlation (95% CL)	ST (Difference, in cm/s)	Correlation (95% CL)	ST (Difference, in cm/s)
Newport, Oregon	0.26 (0.35)	18.3	0.83 (0.75)	11.6	0.83 (0.75)	11.4
Coos Bay, Oregon	0.02 (0.21)	18	0.73 (0.6)	12.6	0.74 (0.6)	12.5
Rogue River, Oregon	−0.2 (0.36)	18	0.77 (0.58)	11.9	0.78 (0.58)	11.5

[a]Only the meridional component of the velocities is considered. First column, name of nearest location; second column, geostrophic velocities estimated from altimetry-only SSH are compared to ADCP currents; third column, geostrophic velocities estimated from the merged product between satellite and tide gauge SSH are compared to the ADCP currents; fourth column, as in the third column but the 10m depth Ekman current is added to the geostrophic velocities. AVISO, Archiving, Validation, and Interpretation of Satellite Oceanographic data; SSH, sea surface height.

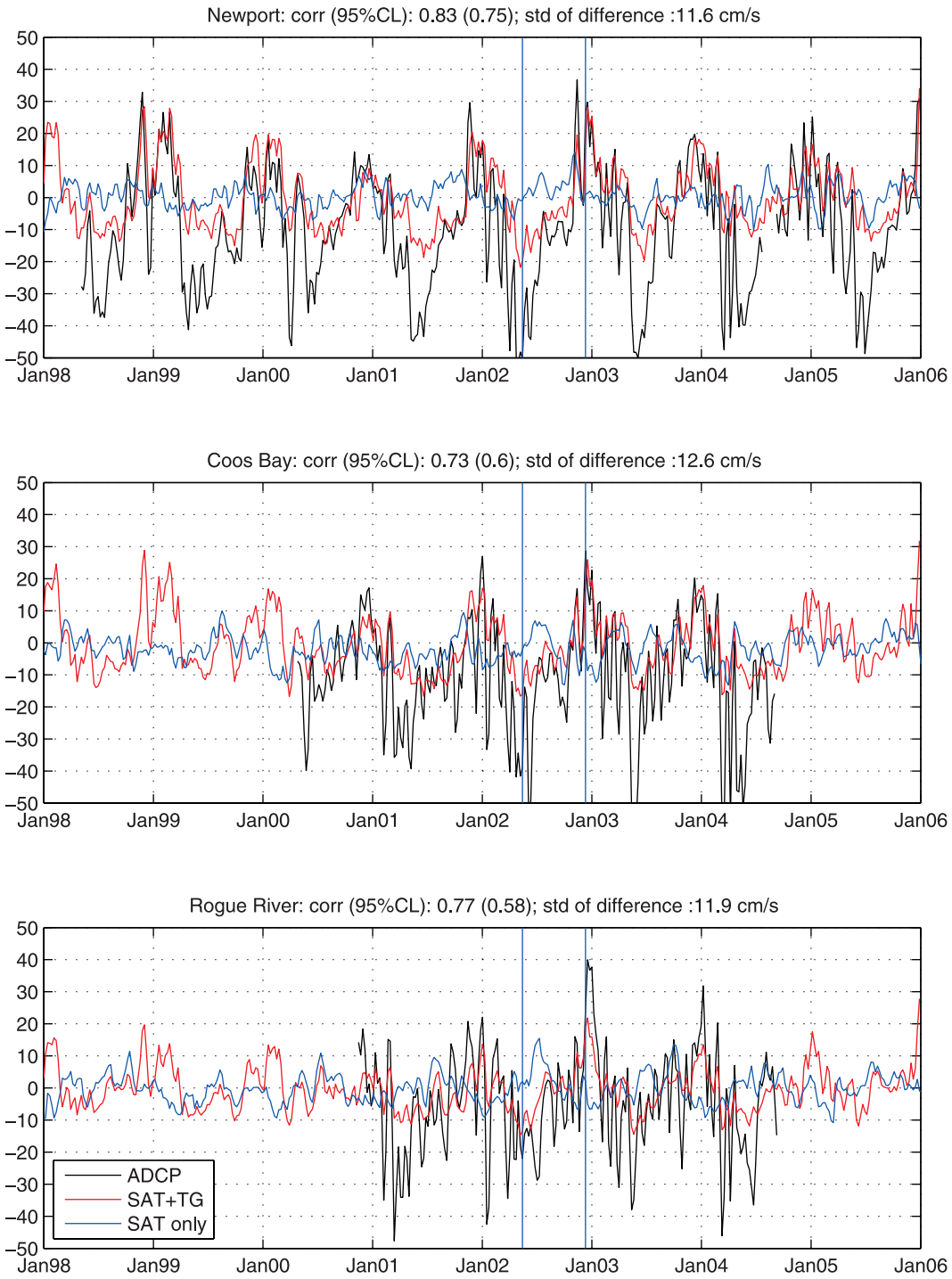

Figure 6. Meridional components of the geostrophic velocities (cm/s) obtained at (top) Newport, (middle) Coos Bay, and (bottom) Rogue River mooring sites from the interpolation of the satellite with the TG SSHs (red line), as measured by the ADCPs at 10 m depth (black line) and as estimated using AVISO SSH altimeter data only (blue line). The titles in Figure 6 (top), Figure 6 (middle), and Figure 6 (bottom) indicate the location of each mooring, the correlation coefficient, 95% CL, and the standard deviation of the difference between alongshore velocities estimated from TG-altimeter SSHs and the ADCP time series. Vertical blue lines indicate the dates used to produce Figures 4 and 5.

become insignificant at the 95% CL (Table 3). This result indicates that the inclusion of the TGs clearly improves the gridded SSHs in the nearshore region.

[29] The highest differences between geostrophic currents estimated from the gradients of SSH produced by merging TG and altimeter data is observed during summers (Figure 6), when the altimeter-TG combination underestimates the

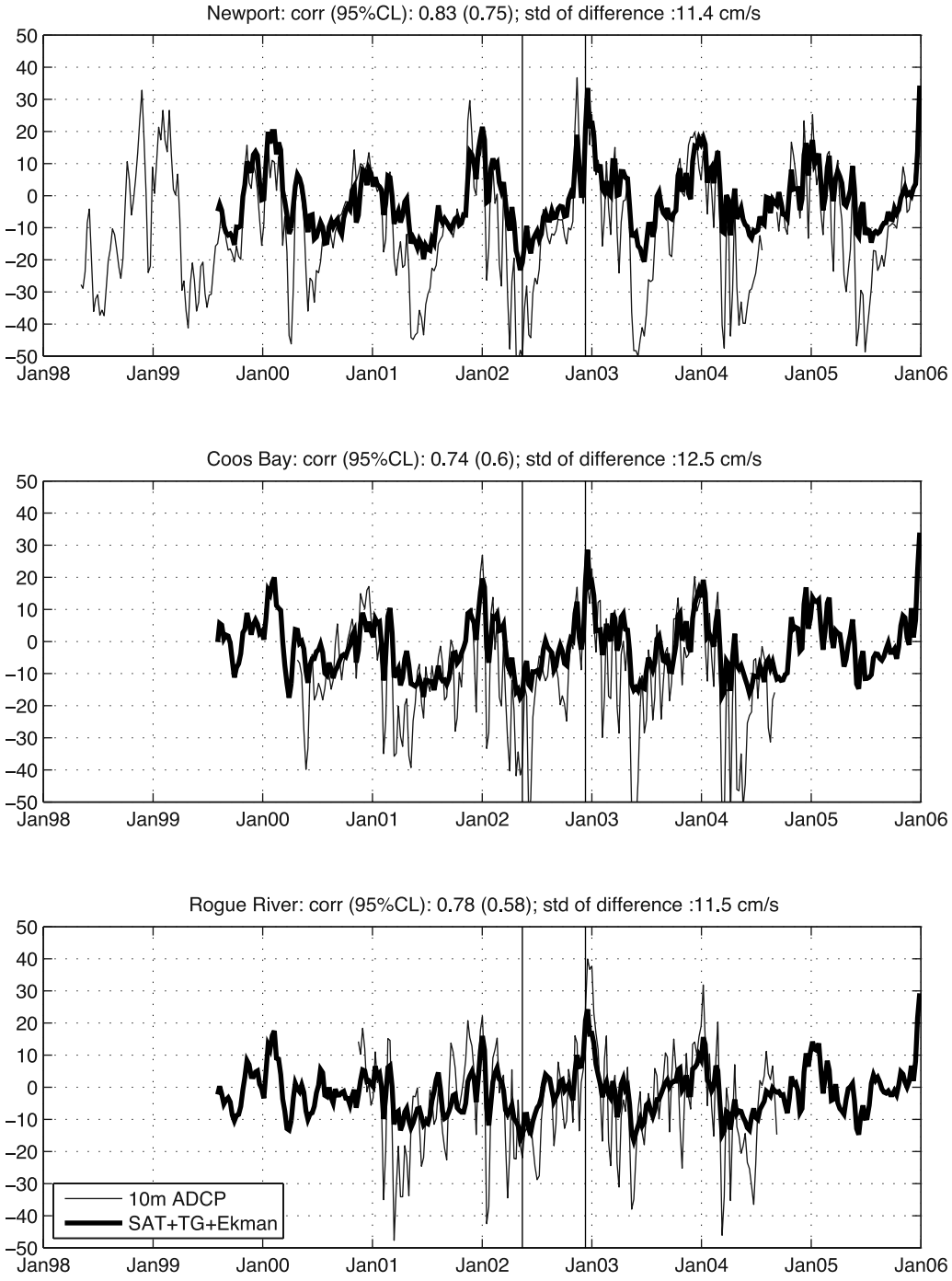

Figure 7. As in Figure 6, after adding the meridional component of the Ekman currents to the merged altimeter-TG SSH time series. AVISO geostrophic time series are not reproduced. Ekman currents are estimated using QuikSCAT winds.

southward velocities at 10 m depth. If the summer periods (21 July to 21 September) are not considered, the standard deviation of the differences decreases to 9.2 cm/s for Newport (South Beach), 9.5 cm/s for Coos Bay and 10.9 cm/s for Rogue River. We explore these differences in several ways in the following subsections.

4.2. Adding Ekman Currents

[30] In situ current measurements at 10 m depth as measured by ADCPs are directly affected by the forcing of the winds. Wind forcing causes a surface Ekman current that is estimated according to the following formula [*Ekman*, 1905] for the meridional component (neglecting the time dependence and considering a nonfinite depth):

$$V_{ekm} = \frac{1}{\rho \cdot d \cdot f} \cdot e^{\frac{z}{d}} \cdot \left[(\tau_y - \tau_x) \cdot \cos\left(\frac{z}{d}\right) + (\tau_x + \tau_y) \cdot \sin\left(\frac{z}{d}\right) \right]; \quad (3)$$

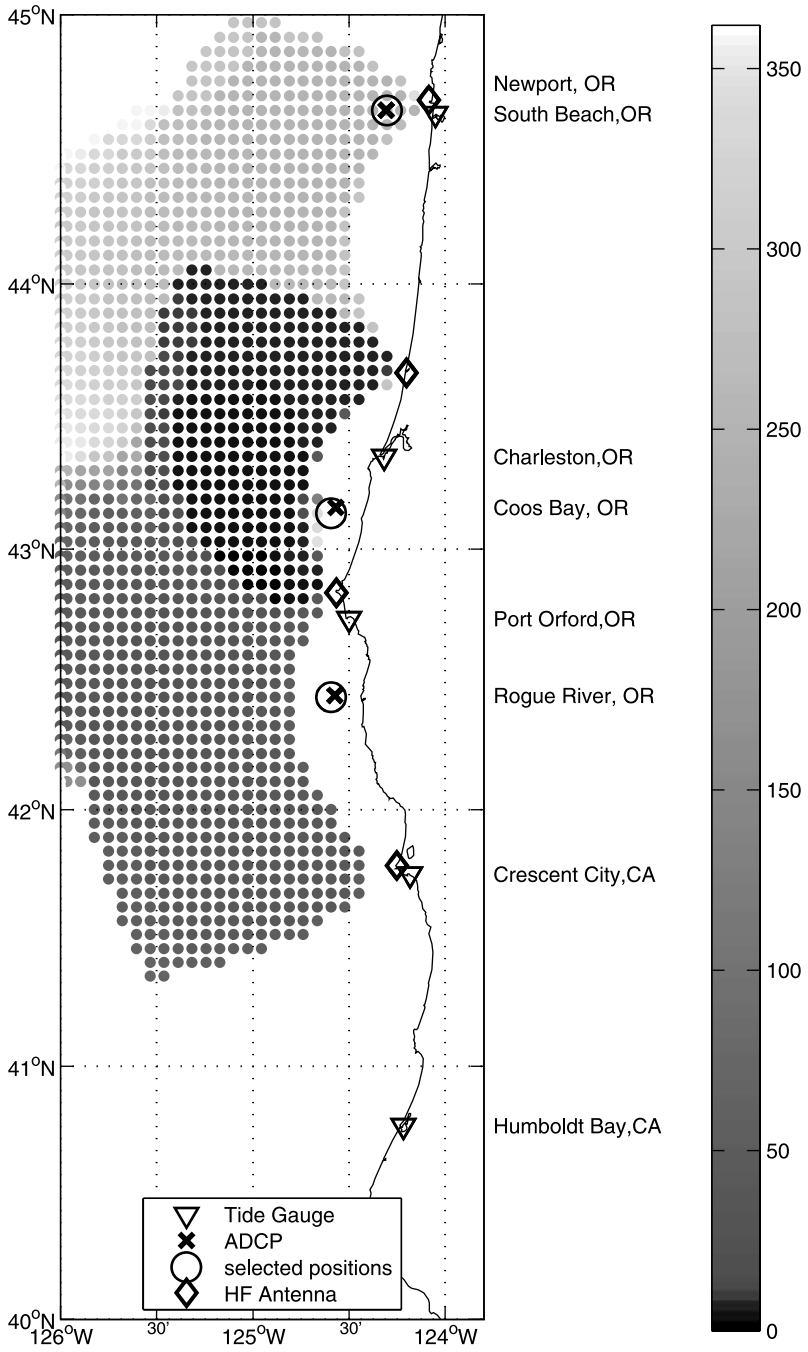

Figure 8. Spatiotemporal coverage of the surface currents mapped by HF measurements during 2002 using 6-hour averages of the data. Gray-filled dots indicate the number of missing data in days, following the vertical bar on the right. Position of the TGs (inverted triangles), ADCPs (crosses), HF antennas (diamonds), and the selected positions (circles) from where time series of HF measurements were extracted to compare with the ADCPs' measurements are indicated.

where z is the vertical coordinate (zero at the surface, positive upward), τ is the surface wind stress (the subscript indicates the component) ρ is the density of seawater, f is the Coriolis parameter and d is the Ekman depth, i.e., the depth at which the amplitude of the current forced only by wind stress decays by a factor of 1/e.

[31] To add the Ekman current at 10 m depth to the geostrophic current previously estimated, we need an estimate of the Ekman depth, of the wind stress and of the density. We use the wind stress as computed from QuikSCAT (see section 2.4), a fixed value of density of 1025 Kg/m^3 and a fixed Ekman depth of 15 m. The latter is a critical parameter and possible temporal variations of this parameter are discussed in section 5.1. The meridional component of the sum of the geostrophic plus 10 m Ekman current is compared to the meridional component of the current measured at 10 m by the ADCP in Figure 7, and correlations are displayed in Table 3. Correlations and

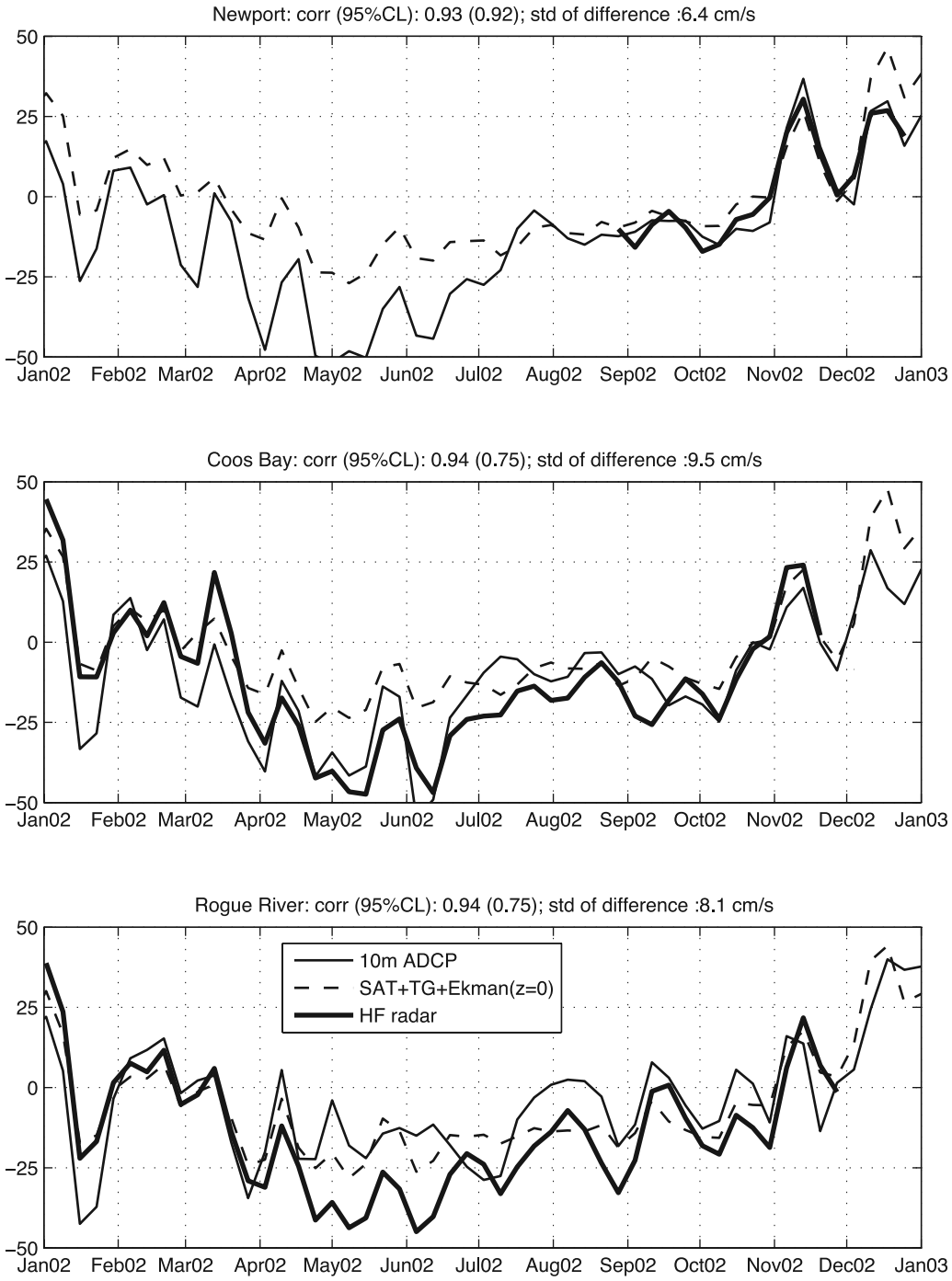

Figure 9. ADCP (thin line) and geostrophic plus Ekman currents (dashed line) (cm/s) as in Figure 7. The bold line indicates the meridional component of the surface velocities (cm/s) as estimated from HF measurements. The correlation, CL, and standard deviation of the difference between the HF measurements and the geostrophic plus Ekman velocities are indicated for (top) Newport, (middle) Coos Bay, and (bottom) Rogue River.

standard deviations of the differences show very small changes (Table 3), indicating a very slightly improved agreement between the two time series. More general discussions of the combination of satellite-derived geostrophic and Ekman velocities for global surface current coverage are presented by *Johnson et al.* [2007] and *Sudre and Morrow* [2008].

4.3. Comparison With HF Measurements

[32] We examined HF surface current data collected during 2002, with durations of up to 1 year, depending on location (Figure 8). Regions where site geometry produces high uncertainty in one of the velocity components (high Geometric Dilution of Precision, GDOP, generally near the

Table 4. Correlations and Standard Deviations of the Differences Between Velocities Estimated From SSH and HF Measurements and ADCP Measurements[a]

	Vgeo+Ekman (z = 0) Versus HF Measurements		Vgeo+Ekman (z = 10 m) Versus ADCP		Vgeo Versus HF Data (No Ekman)	
Name of Location	Correlation (95% CL)	SD (Difference, in cm/s)	Correlation (95% CL)	SD (Difference, in cm/s)	Correlation (95% CL)	SD (Difference, in cm/s)
Newport, Oregon	0.93 (0.92)	6.4	0.92 (0.85)	7.7	0.92 (0.84)	8.1
Coos Bay, Oregon	0.94 (0.75)	9.5	0.82 (0.62)	12	0.8 (0.67)	12.4
Rogue River, Oregon	0.94 (0.75)	8.1	0.74 (0.55)	10.5	0.69 (0.55)	11.1

[a]Only the meridional component of the velocities is considered. Geostrophic velocities (Vgeo) are estimated from the merged product between satellite and tide gauge SSH. First column, name of nearest location; second column, surface (z = 0) Ekman currents are added to the Vgeo and compared to the HF currents; third column, Ekman currents at 10m depth (z = 10) are added to the Vgeo and compared to the ADCP currents at 10 m depth; fourth column, Vgeo are compared to the HF currents without adding any Ekman current.

coast between sites and very far from the coast) were eliminated (Figure 8). The results of the comparison between the HF velocity time series and our geostrophic velocities are displayed in Figure 9 and summarized in Table 4. Because HF systems measure the very near surface currents, typically 1–2 m in depth [*Stewart and Joy*, 1974; *Fernandez et al.*, 1996], we estimate the Ekman currents at the surface, prior to adding them to the geostrophic currents estimated from the SSH. Correlation coefficients are 0.93 for Newport (South Beach) and 0.94 for Coos Bay (Charleston) and Rogue River (Port Orford, Cape Blanco), with standard deviations of the differences lower than 9.5 cm/s for the three cases. This indicates very good agreement between the HF measurements and velocities estimated from our SSH fields with the addition of the Ekman component. When the Ekman component is not included, correlations decrease and standard deviations of the differences increase by at least 1.7 cm/s (Table 4). The highest difference caused by adding the Ekman component is found at Rogue River, indicating that the direct effect of the wind forcing may be more significant at that location. Although the standard deviation of the difference at Newport (South Beach) is low (6.4 cm/s, including Ekman), it should be noted that the HF surface currents time series at Newport starts only at the end of August 2002. This is after the summer period of southward currents associated with the upwelling-favorable winds, which produces the largest differences between current estimates from the altimeter-TG combinations and the in situ or HF measurements.

[33] The correlation coefficients and standard deviations of the differences between ADCP data at 10 m and our geostrophic velocities (including the Ekman current at 10 m depth) are also indicated in Table 4, using data only from the same period covered by the HF measurements. Both correlation coefficients and standard deviations of the differences indicate that the correspondence is better between our altimeter-TG estimates and HF surface velocities than between our velocities and ADCP data. Thus, the comparison indicates that our velocities (including the surface Ekman component) are better at representing the very surface currents.

[34] Results summarized in Table 4 clearly reflect what can be observed visually (Figure 9) in the time series of Coos Bay and Rogue River. In particular, our velocities and HF measurements are almost identical in the first part of the year (up to mid-April 2002 for Rogue River). In mid-January 2002, the time series at Coos Bay and Rogue River indicate the presence of a southward current whose signature is more pronounced in the ADCP data than in the HF data. If we assume that both HF and ADCP data represent accurate measurements of the currents, this indicates a strong vertical shear between the HF surface currents and the subsurface currents (10 m depth) during this event. Between mid-April and mid-June, the situation is different: at Coos Bay our velocities clearly underestimates the amplitude of the southward current, while at Rogue River the highest difference is between ADCP and HF measurements. During the rest of the year the three curves have a similar behavior: SSH derived velocities more closely match the HF surface current maps rather than the ADCP velocities.

5. Discussion and Conclusions

[35] Geostrophic velocities estimated from a merged product between satellite and tide gauge (TG) SSH have been compared with ADCP and HF currents in the above section. The results can be summarized as follows:

[36] 1. In regions within 40–50 km of the Oregon coast, the available globally gridded SSH fields (derived from standard along-track altimeter data) produce alongshore geostrophic currents that do not correlate well with measured, in situ velocities. This is primarily attributed to the lack of reliable along-track data near land. At least 75% of the along-track altimeter SSH data are flagged by AVISO as invalid in a region that extends up to 37 km from the coast, resulting in extrapolation of the offshore SSH data into the coastal band. This extrapolation lacks the measurements or dynamics needed to resolve horizontal variability in the SSH and current fields in the coastal ocean. The flagging of data as unreliable is due to intrinsic difficulties in tracking the reflected altimeteric radar signal near land and in the corrections applied to the altimeter data when land is nearby (see below).

[37] 2. Interpolation between the more reliable altimeter SSH data from the offshore region and SSH data from TGs along the coast results in geostrophic currents that correlate well (at the 95% CL) with in situ measurements of the alongshore currents, even when using simple linear interpolations between measured offshore and coastal data.

[38] 3. The largest differences occur systematically when upwelling-favorable (equatorward) winds drive a strong southward jet along the coast.

[39] 4. When the Ekman current components are estimated and added to the geostrophic currents, comparisons to the 10 m deep ADCP velocities are only slightly improved. The

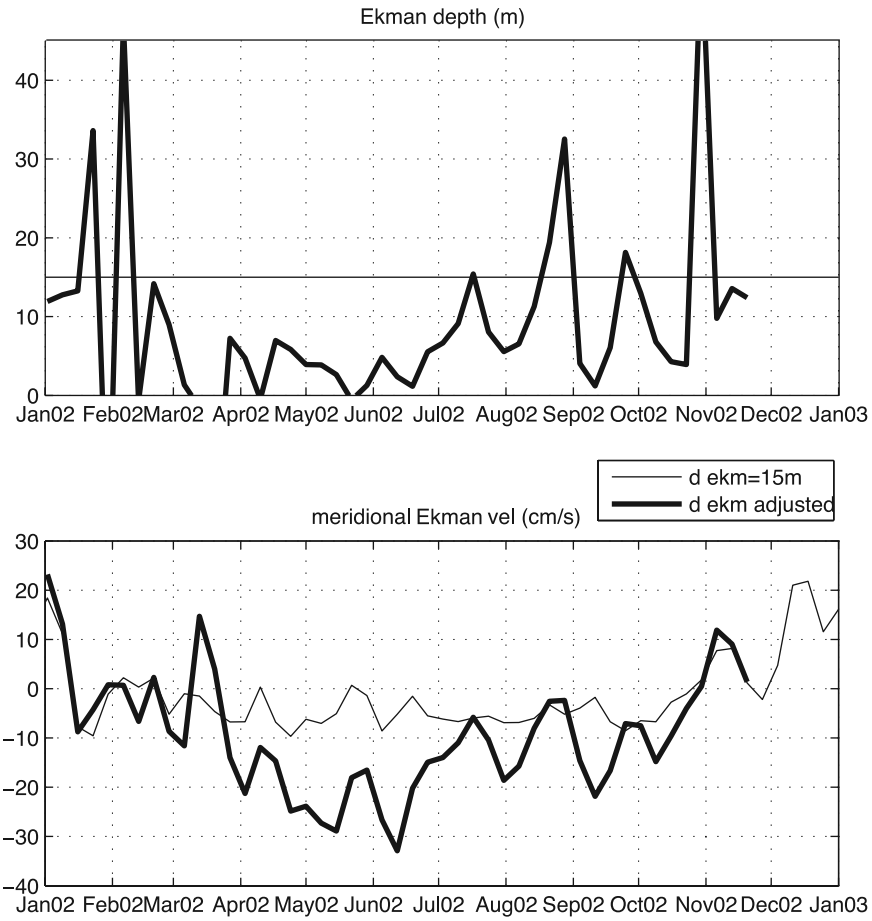

Figure 10. At Coos Bay, (top) Ekman depth (m) and (bottom) meridional Ekman velocities (cm/s) as estimated from equation (5) (bold line) and as calculated using a constant Ekman depth of 15 m (thin line).

Ekman components make a more significant contribution when compared to the HF surface current measurements.

[40] We interpret the first two points above to suggest that additional, realistic SSH data from within the coastal band can dramatically improve the gridded SSH and velocity fields in the same region. Although we use coastal tide gauge data in our region, improved retrievals of along-track altimeter data closer to the coast would provide a more general solution to the problem, as discussed below. The third and fourth points above suggest that horizontal and vertical gradients of surface currents are more variable in time and space in coastal regions than assumed in our simple example. Below we discuss these gradients, starting with the vertical gradients of the Ekman currents and continuing with horizontal gradients of currents and SSH. This leads to the discussion of improved retrievals of the along-track SSH data, which is the best hope for coastal altimetry.

5.1. Estimates of Ekman Currents and Ekman Depths

[41] Our estimates of the Ekman currents assume a constant Ekman depth and a constant density. In reality, these two parameters are not constant in space or time. The density of seawater changes considerably in the region considered here, because of the sporadic presence of fresh water from the Columbia River in a surface layer. These fresher surface layers only reduce the surface density by less than 1% of its mean value [*Huyer*, 1977], producing little direct effect on the Ekman current estimation (see equation (3)). However, they can provide a buoyant surface layer which requires more energy to mix vertically, reducing the Ekman depth and resulting in the concentration of the wind's momentum in a shallow layer with greatly enhanced surface currents. Estimates of surface currents from the HF measurements can be substituted for the surface Ekman currents and combined with estimates of the wind stress (from QuikSCAT) and geostrophic currents (from altimeter SSH) to estimate the "empirical" Ekman depth (d):

$$V_{ekm}(z=0) = \frac{1}{\rho \cdot d \cdot f} \cdot \left(\tau_y - \tau_x\right); \tag{4}$$

$$d = \frac{\left(\tau_y - \tau_x\right)}{\rho \cdot f \cdot \left(V_{HF} - V_{geo}\right)}; \tag{5}$$

[42] Results of the empirical estimation of Ekman depth (Figure 10 (top)) are roughly consistent with the 15 m depth assumed during winter and autumn but show a lower value during spring and summer. Thus, use of a shallower Ekman depth during spring and summer would result in stronger

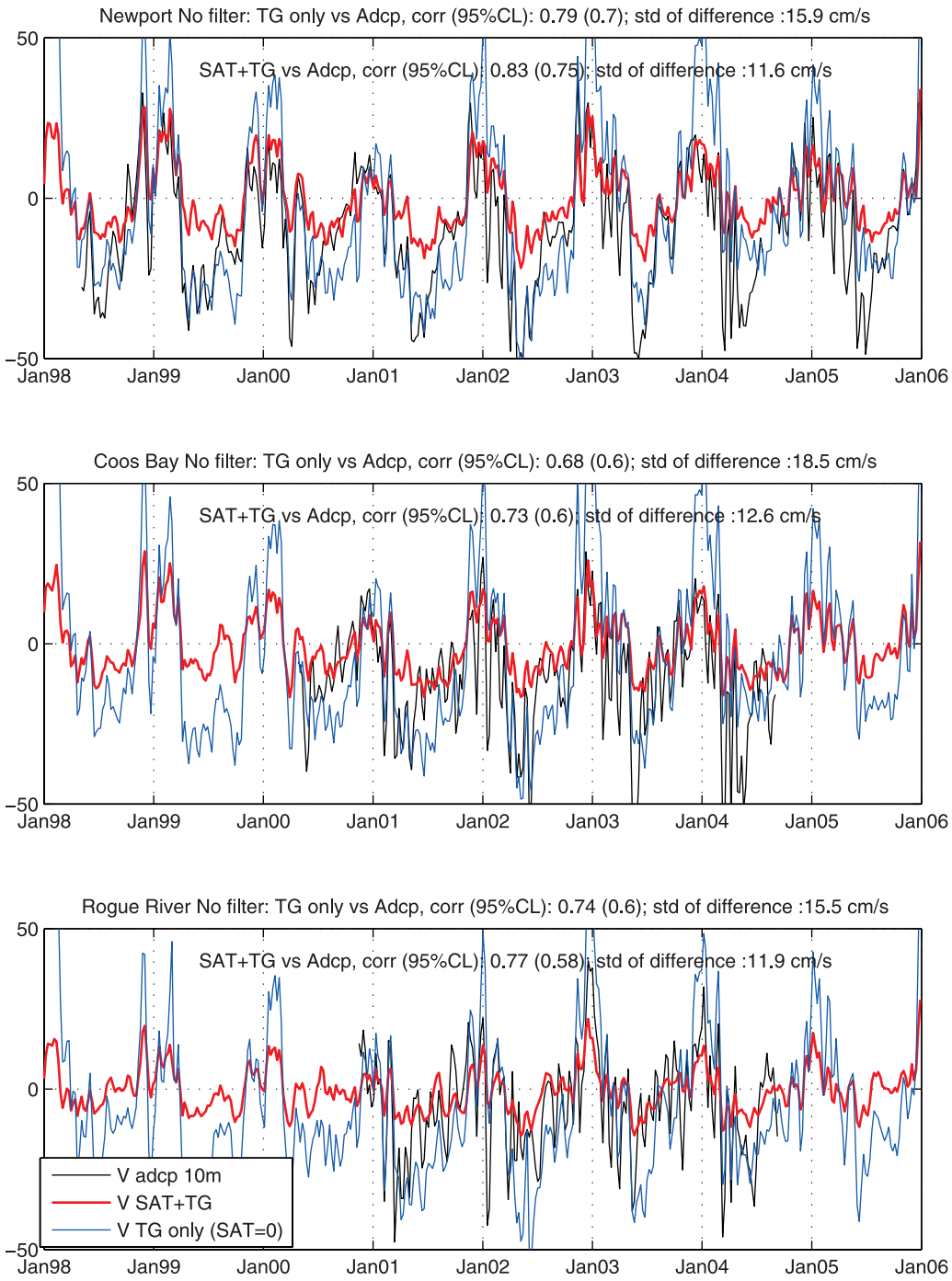

Figure 11. Comparison of alongshore currents (cm/s) at (top) Newport, (middle) Coos Bay, and (bottom) Rogue River. TG-only (blue line) currents are estimated fixing the SSH (z = 0) 40 km offshore, i.e., only considering the forcing of the TG. The result obtained by merging TG and satellite data and as estimated by the ADCP at 10 m depth are displayed with red and black lines, respectively. Correlations and standard deviations of the difference obtained between time series are presented in Table 5.

southward currents (Figure 10 (bottom)) that would better match the observed currents. This would require independent estimates of Ekman depths, which cannot be obtained from satellites but could come from several other sources. Seasonal changes in Ekman depths could be specified from climatologies of density profiles and mixed layer depths. For example, better estimates of temporally and spatially varying density structure could be made from moorings and autonomous vehicle measurements, available from the coastal monitoring systems planned by the U.S. Integrated Ocean Observing System (IOOS). Even more complete estimates of the 3-D density fields could come from coastal circulation models run in the IOOS systems. However, these models will eventually assimilate the altimeter SSH and HF

Table 5. Correlations and Standard Deviations of the Difference Between TG-Only, SAT+TG, and ADCP Velocity Time Series When They Are Unfiltered, Low-Pass Filtered, and High-Pass Filtered[a]

		Unfiltered		Low-Frequency		High-Frequency	
Location	Instruments Compared	Correlation (95% CL)	SD (Difference, in cm/s)	Correlation (95% CL)	SD (Difference, in cm/s)	Correlation (95% CL)	SD (Difference, in cm/s)
Newport	SAT+TG versus ADCP	0.83(0.75)	11.6	0.82(0.8)	9.6	0.77(0.2)	6.4
Newport	TG-only versus ADCP	0.79(0.7)	15.9	0.75(0.8)	16.9	0.76(0.2)	6.6
Coos Bay	SAT+TG versus ADCP	0.73(0.6)	12.6	0.77(0.8)	8.4	0.7(0.29)	9.2
Coos Bay	TG-only versus ADCP	0.68(0.6)	18.5	0.73(0.8)	16	0.71(0.2)	8.4
Rogue River	SAT+TG versus ADCP	0.77(0.58)	11.9	0.82(0.8)	7.3	0.75(0.3)	9.4
Rogue River	TG-only versus ADCP	0.74(0.6)	15.5	0.8(0.88)	13	0.75(0.3)	7.8

[a]SAT+TG, merged product between satellite and tide gauge sea level anomaly.

surface velocity fields, producing more realistic velocity fields that make the calculation of Ekman and geostrophic velocities from the satellite data a moot point.

5.2. Estimation of the Alongshore Current by TGs Only: Variability in Large-Scale Coastal SSH Gradients

[43] It is natural to ask how much of the alongshore velocity and transport in the gap region is contributed by SSH variations in the tide gauge record alone, compared to the combination of tide gauges and offshore altimeter SSH fields. *Huyer et al.* [1978] found that alongshore currents over the Oregon shelf vary simultaneously with tide gauge SSH measurements at the coast. Assuming linear or exponential decays of the sea level from the coast, *Kundu et al.* [1975] and *Huyer et al.* [1978] estimate an offshore length scale L over which the geostrophic velocities correctly approximate the alongshore currents. *Huyer et al.* [1978] found that L is larger in winter than in spring and summer, the value depending on the approximation considered (linear or exponential). Considering the linear approximation, values are 52 km for winter, between 17 and 35 km for spring and 30–40 km for summer [*Huyer et al.*, 1978]. This seasonal variability is consistent with changes in the Rossby radius of deformation, which is minimum during summer and maximum in winter, because of seasonal changes in the stratification and mixed layer depth.

[44] We test these relationships with the present data, using a constant offshore length scale (L) and a SSH profile that decays linearly from the value measured at the tide gauge to 0 cm at L = 40 km. We compare the resulting geostrophic currents to those produced by the TG and altimeter combination and those measured by the ADCPs located over the shelves at Newport (8 years of data), Coos Bay (5 years of data) and Rogue River (4 years of data). Differences between the TG-only and ADCP currents are, in general, small in spring-summer and large in winter, consistent with results from *Huyer et al.* [1978]. The large overestimates of poleward currents by the TG-only time series in winter are consistent with the fact that the effective L is larger in winter and values of SSH are not zero 40 km offshore. The altimeter provides better estimates of SSH at 40 km offshore during winters. The underestimates of equatorward currents by the combination of TG and altimeter data in spring and early summer are due to the underestimate of the SSH gradients associated with the upwelling jet. The true SSH gradients in summer occur over much shorter distances across the jet (see section 5.3). When the strong SSH gradient associated with the jet moves offshore of the shelf and current meter in late summer and autumn [*Strub and James*, 2000], the combination of TG and altimeter data produces a better estimate of the measured alongshore current than the 40 km linear gradient using only the TG data.

[45] The above comparisons are quantified by values of the standard deviations of the difference between the ADCP and calculated alongshore velocities, along with their correlations. At Newport, with the longest time series, our altimeter-TG estimates of SSH and geostrophic currents produce values of 11.6 cm/s (standard deviation of difference) and 0.83 (correlation coefficient, see Figure 6 and Table 3). Use of the TG only SSH with L = 40 km results in values of 15.9 cm/s and 0.79 (see Figure 11 and Table 5). Thus, using the altimeter data on the offshore boundary of the 40 km gap region improves the results. The same tendency is found at Rogue River and Coos Bay, i.e., correlations are very similar but standard deviations of the differences present lower values when TGs are merged with satellite SSH data (Table 5).

[46] Using the measured ADCP time series of alongshore velocities, we can find an optimal value of L to use in the TG-only calculations, to best match the measurements. The standard deviation of the difference between the measured ADCP alongshore currents at 10 m depth and the TG only calculation decreases exponentially as L increases to a distance of 70 km from the coast, increasing slowly for L larger than 70 km. With L = 70 km, the standard deviation of the difference between the ADCP and TG-only calculation is 11.3 cm/s and the correlation coefficient is the same as with L = 40 km. The decrease in standard deviation of the differences is due to a decrease in overestimation of alongshore velocities in winter and a smaller increase in underestimates of velocities in summer.

[47] Although correlations of low-frequency signals in the time series are dominated by seasonal cycles, significant correlations are found at higher frequencies (periods of weeks). To demonstrate this, we estimate the correlations between unfiltered, low-pass filtered and high-pass filtered time series of the SAT+TG and TG only versus ADCP data, respectively. Time series are low-pass filtered using a 90-day period as the cutoff frequency, separating seasonal (and longer) variability from intraseasonal variability. The high-frequency time series are constructed as the difference between the unfiltered and the low-pass filtered time series. Results (see Table 5) indicate that while correlation values are similar for low- and high-frequency time series, only the high-frequency signals are significantly correlated (well above the 95% significance level). The lack of significance

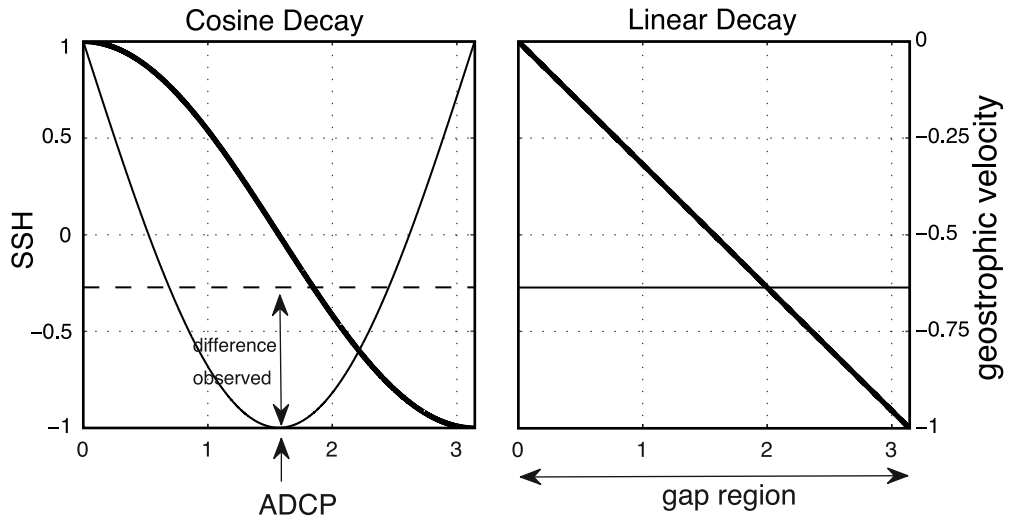

Figure 12. Schematic representation of SSH (bold lines) and corresponding geostrophic velocities (thin lines) of (left) a cosine-like decay of SSH and (right) a linear decay in the gap region. The position of the ADCP is indicated.

for the low-frequency signals is due to the fact that they are dominated by the seasonal cycles, which have a low number of degrees of freedom over the 4–8 year time series (with lower significance levels for high correlations).

[48] Table 5 also shows that the standard deviations of the differences of the unfiltered and low-pass filtered time series are lower (by at least 3.6 cm/s) when the satellite information is interpolated to the TGs rather than when the TG only are considered. This supports the previous conclusion that the altimeter data provides offshore information that compensates for the seasonally changing length scale for the offshore decay of the coastal SSH, as measured by the tide gauges. The contributions of the offshore altimeter data are more important on the seasonal and longer timescales than on the intraseasonal timescales. This is demonstrated by the fact that the standard deviations of the difference for the high-frequency components present almost no differences (with or without altimeter data). This reflects the fact that present altimeters do not adequately sample synoptic and intraseasonal timescales. It also emphasizes the need to integrate altimeter data with observations from instruments that do sample higher-frequency timescales (tide gauges, coastal radars, moorings, etc.) for coastal observing systems.

5.3. Interpolation of SSH in the Gap Region: Variability in Small-Scale Coastal SSH Gradients and the Path Forward for Improved Coastal Fields

[49] The above discussion suggests that the greatest source of error in the new estimates of alongshore velocity may come from our use of a linear interpolation of SSH in the gap region. In situ observations show that during upwelling favorable winds the dynamic height does not decay linearly in the gap region. Instead, the slope of the SSH in the gap region is concentrated, on average, around a narrower region of maximum slope [*Fleischbein et al.*, 2005, Figure 19], and the equatorward alongshore surface flow is often concentrated into a current jet [e.g., *Kosro*, 2005], whose core location changes with time. Averaged over weeks to months, the slope of the SSH resembles a "cosine-like" decay of SSH, with maximum slope and a strong jet in the middle of the gap region, as depicted schematically in Figure 12. This observation was, in fact, the motivation for the location of the ADCP mooring at midshelf off Newport.

[50] At any given time, however, even narrower coastal jets, filaments and other small-scale structures in SSH and velocity are found routinely in coastal regions [*Kosro*, 2005; *Barth et al.*, 2005a, 2005b; *Fleischbein et al.*, 2005]. An example is shown from the Oregon coast during June 2005, in Figure 13. A band of colder SST values is seen next to the coast south of 45°N on 29 June. Two altimeter tracks are shown (straight lines) ascending from SW to NE (27 June) and descending from the NW to SE (28 June). SSH data from these tracks are recovered by substituting a model-derived "wet troposphere atmospheric correction" for the standard correction from the onboard microwave radiometer, which does not produce usable data east of ~125°W (see below). Along the descending (NE–SW) track, SSH values (the fluctuating lines) drop approximately 12 cm as the altimeter approaches the coast at ~44.7°N, 124.8°W, and drop again ~25 cm near 44.3°N, 124.4°W. The second, larger drop in SSH occurs approximately where the altimeter track crosses from warmer to colder water. The SSH values represent the vertically integrated specific volume of the water column (here controlled primarily by the temperature), similar to dynamic heights. From past measurements, we expect a strong jet along the SST/SSH front. The smaller drop in SSH, farther offshore, represents another subsurface density front that is covered by a surface layer of warm SST and should correspond to a weaker jet. These fronts demonstrate the true nature of the SSH and current fields at any given time, which are poorly resolved by a linear gradient of SSH between the coast and the offshore region. However, the geostrophic alongshore transport integrated across the gap is accurately portrayed, regardless of the shape of the SSH field in the gap region, and the linear interpolation

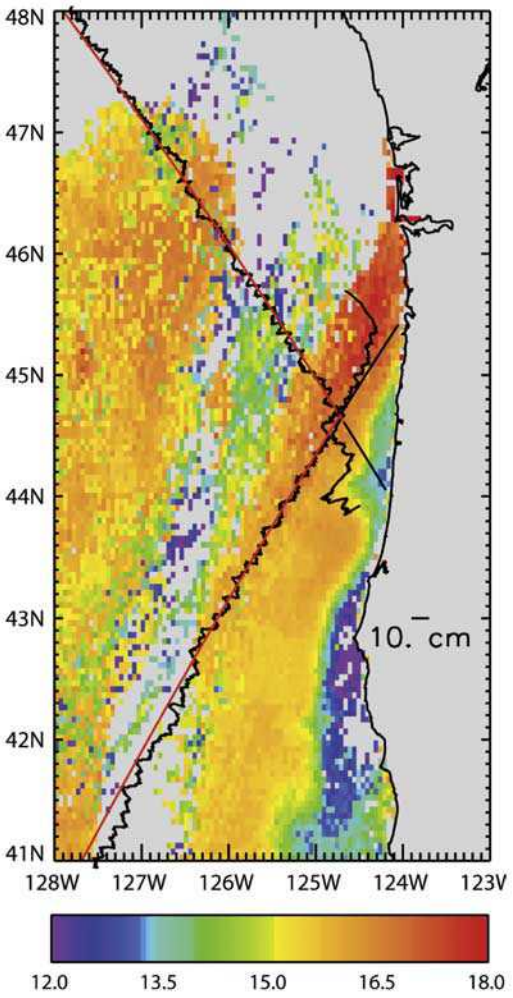

Figure 13. SST (colors) from the Advanced Very High Resolution Radiometer and along-track SSH from the Jason-1 altimeter during 27–29 June 2005. A wet troposphere correction from the European Center for Medium-range Weather Forecasting model has been substituted for the standard correction to retrieve SSH data east of 125°W. Clouds are indicated by gray and speckled patterns in the offshore and northern regions. The region next to the coast south of the Columbia River (46.3°N) is relatively cloud free. Altimeter track paths are the straight lines (red indicates offshore, and black indicates east of the track crossover at 124.7°W); along-track SSH values are shown by the solid traces fluctuating above and below the tracks (10-cm-scale distance shown over land). Low-SSH values are indicated when the SSH traces are offshore (left) of the tracks. Sharp drops in SSH (∼12 cm and ∼25 cm) are seen along the track moving from NW to SE at ∼44.7°N, 124.8°W and 44.3°N, 124.4°W, respectively.

provides a large increase in skill compared with the original, extrapolated AVISO product.

[51] Our interpolation of SSH between valid offshore altimeter data and coastal tide gauges represents a first step in improving the SSH fields in coastal regions. It primarily demonstrates that more realistic SSH data from within the coastal region are able to improve altimeter estimates of SSH and surface currents within approximately 40 km of land. The use of tide gauge data and an assumed shape for the interpolated SSH profile (linear, cosine or otherwise) across the coastal gap is a weakness of the present analysis, motivated by the lack of measurements in the gap region interior. For many coastal locations, an additional limitation for this technique is the lack of a relatively dense array of well-maintained tide gauges, with long and consistent time series.

[52] The more general solution to the problem of obtaining improved fields of SSH in coastal regions requires better methods for retrieving the along-track altimeter SSH data in those regions. This will replace the use of tide gauges, with global coverage to within approximately 5 km of land. However, modification are needed for the methods used to retrieve the altimeter's reflected radar signal and to estimate "corrections" to the path delay caused by atmospheric constituents and surface effects. Close to the coast (10–20 km), land contaminates the actual reflected altimetric radar signal. Advanced methods for tracking the reflection point of the radar signal from the ocean and land surfaces are needed, as described by *Fenoglio-Marc et al.* [2007]. Farther from the coast, the large footprint of the onboard microwave radiometers used to estimate the wet tropospheric path delay (because of vertically integrated atmospheric water vapor) intersects land and creates a data gap within approximately 50 km of land. Alternative estimates for the wet tropospheric correction are provided by atmospheric models [*Madsen et al.*, 2007], as used in Figure 13, although they may not resolve sharp gradients in atmospheric moisture, associated with fronts near the coast. Modified algorithms for the onboard microwave radiometer are being explored, as described by *Desportes et al.* [2007].

[53] Algorithms to correct for these and other atmospheric and surface effects in coastal regions are the subject of several international initiatives, including ALTICORE [*Vignudelli et al.*, 2008; *Bouffard et al.*, 2008] (information available at www.alticore.eu), COASTALT [*Cipollini et al.*, 2008] (data are available at www.coastalt.eu), and PISTACH [*Lambin et al.*, 2008]. Improvements in methods for coastal altimetry are also being discussed in an ongoing series of workshops [*Smith et al.*, 2008]. Our results demonstrate that inclusion of more realistic SSH data (from tide gauges, altimeter tracks or other sources) in producing gridded SSH fields will result in improved estimates of surface currents in these coastal regions, where society's use of the ocean continues to increase.

5.4. Summary

[54] The present work shows that the combination of SSH data from tide gauges and satellite altimeter fields improves the altimeter SSH fields within 40–50 km of the coast and increases the accuracy of the alongshore surface velocities derived from those fields. We also point out that compact structures such as coastal jets are only partially represented using the linear interpolation techniques employed here, causing higher differences between SSH-derived velocities and in situ measurements in summer over the shelf off Oregon. These jets are narrower than can be represented by a linear interpolation of SSH from 40 km offshore to the tide gauges at the coast. To improve the representation of the velocity structure in the 40 km next to the coast, methods

must be found to retrieve the actual along-track altimeter SSH data in that region. These data can then be used in two ways:

[55] 1. They can be used as inputs to advanced gridding techniques, such as employed by AVISO, to produce more realistic SSH fields. Surface velocity fields can be produced from the SSH fields, with or without the addition of Ekman components [*Johnson et al.*, 2007; *Sudre and Morrow*, 2008].

[56] 2. The same SSH data (either along-track or gridded) can be assimilated into dynamical models of coastal ocean circulation (A. L. Kurapov et al., Representer-based analyses in the coastal upwelling system, submitted to Dynamics of Atmospheres and Oceans, 2008). However, our results show that the presently available gridded SSH fields, without the inclusion of more realistic SSH data (from tide gauges or improved along-track altimeter data), do not accurately represent details of the circulation within 40–50 km of the coast and should not be assimilated into coastal models.

[57] Ignoring spatial details of the coastal circulation, for regions with narrow shelves, the spatially integrated geostrophic alongshore transport in the region within 40 km of the coast depends only on the difference of SSH across that region (not on the particular shape of the SSH). Thus, the techniques described here can be used to construct a 15 year index of the alongshore transport within ~40–50 km of the coast, anywhere that a sufficiently long record of SSH from a well-maintained tide gauge exists. This index may be used for studies of climatic variability in water mass characteristics, plankton species, etc., caused by changes in alongshore transports.

[58] **Acknowledgments.** Support for M.S., P.T.S., and P.M.K. was provided by NOAA/NESDIS through the Cooperative Institute for Oceanographic Satellite Studies (NOAA grant NA03NES4400001) and the U.S. GLOBEC project (NSF grants OCE-0000733, OCE-0000734, and OCE-0000900). Additional support for P.T.S was provided by NASA/JPL (grant JPL-1206714-OSTM). The altimeter products were produced by SSALTO/DUACS (Segment Sol multimissions d'ALTimétrie, d'Orbitographie et de localization précise/Data Unification Altimeter Combination System) and distributed by AVISO with support from CNES (Centre National de la Recherche Scientifique). We thank S. Ramp (NPS) and B. Hickey (UW) for making available processed measurements from their GLOBEC moorings at Rogue River and Coos Bay, respectively. Comments by three anonymous reviewers and the editor greatly improved the paper. This is contribution 604 of the U.S. GLOBEC program, jointly funded by the National Science Foundation and the National Oceanic and Atmospheric Administration.

References

Allen, J. S. (1975), Coastal trapped waves in a stratified ocean, *J. Phys. Oceanogr.*, *5*, 300–325, doi:10.1175/1520-0485(1975)005<0300:CTWIAS>2.0.CO;2.

Barber, C. B., D. P. Dobkin, and H. T. Huhdanpaa (1996), The Quickhull Algorithm for convex hulls, *Trans. Math. Software*, *22*(4), 469–483, doi:10.1145/235815.235821.

Barrick, D. E., M. W. Evans, and B. L. Weber (1977), Ocean surface currents mapped by radar, *Science*, *198*, 138–144, doi:10.1126/science.198.4313.138.

Barth, J. A., S. D. Pierce, and R. L. Smith (2000), A separating coastal upwelling jet at Cape Blanco, Oregon and its connection to the California Current System, *Deep Sea Res., Part II*, *47*, 783–810, doi:10.1016/S0967-0645(99)00127-7.

Barth, J. A., S. D. Pierce, and R. M. Castelao (2005a), Time-dependent, wind-driven flow over a shallow midshelf submarine bank, *J. Geophys. Res.*, *110*, C10S05, doi:10.1029/2004JC002761.

Barth, J. A., S. D. Pierce, and T. J. Cowles (2005b), Mesoscale structure and its seasonal evolution in the northern California Current System, *Deep Sea Res., Part II*, *52*, 5–28, doi:10.1016/j.dsr2.2004.09.026.

Brink, K. H. (1991), Coastal-trapped waves and wind-driven currents over the continental shelf, *Annu. Rev. Fluid Mech.*, *23*, 389–412, doi:10.1146/annurev.fl.23.010191.002133.

Bouffard, J., S. Vignudelli, M. Herrmann, F. Lyard, P. Marsaleix, Y. Ménard, and P. Cipollini (2008), Comparison of ocean dynamics with a regional circulation model and improved altimetry in the northwestern Mediterranean, *Terr. Atmos. Oceanic Sci.*, *19*, 117–133, doi:10.3319/TAO.2008.19.1-2.117(SA).

Carrère, L., and F. Lyard (2003), Modeling the barotropic response of the global ocean to atmospheric wind and pressure forcing—Comparisons with observations, *Geophys. Res. Lett.*, *30*(6), 1275, doi:10.1029/2002GL016473.

Chelton, D., and M. G. Schlax (2003), The accuracies of smoothed sea surface height fields constructed from tandem satellite altimeter datasets, *J. Atmos. Oceanic Technol.*, *20*, 1276–1302, doi:10.1175/1520-0426(2003)020<1276:TAOSSS>2.0.CO;2.

Cipollini, P., J. Gomez-Enri, C. Gommenginger, C. Martin-Puig, S. Vignudelli, P. Woodworth, and J. Benveniste (2008), Developing radar altimetry in the oceanic coastal zone: The COASTALT project, paper presented at the General Assembly 2008, Eur. Geosci. Union, Vienna, 13–18 Apr.

Cleveland, W. S., and S. Devlin (1988), Locally weighted regression: An approach to regression analysis by local fitting, *J. Am. Stat. Assoc.*, *83*, 596–610, doi:10.2307/2289282.

Davis, R. E. (1976), Predictability of sea surface temperature and sea level pressure anomalies over the North Pacific Ocean, *J. Phys. Oceanogr.*, *6*, 249–266, doi:10.1175/1520-0485(1976)006<0249:POSSTA>2.0.CO;2.

Delaunay, B. (1934), Sur la sphère vide, *Otdelenie Mat. Estestvennykh Nauk*, *7*, 793–800.

Deng, X., and W. E. Featherstone (2006), A coastal retracking system for satellite radar altimeter waveforms: Application to ERS-2 around Australia, *J. Geophys. Res.*, *111*, C06012, doi:10.1029/2005JC003039.

Desportes, C., E. Obligis, and L. Eymard (2007), On the wet tropospheric correction for altimetry in coastal regions, *IEEE Trans. Geosci. Remote Sens.*, *45*(7), 2139–2142, doi:10.1109/TGRS.2006.888967.

Ekman, V. W. (1905), On the influence of the Earth's rotation on ocean currents, *Arch. Math. Astron. Phys.*, *2*, 11.

Fenoglio-Marc, L., S. Vignudelli, A. Humbert, P. Cipollini, M. Fehlau, and M. Becker (2007), An assessment of satellite altimetry in proximity of the Mediterranean coastline, paper presented at 3rd ENVISAT Symposium, Eur. Space Agency, Montreux, Switzerland.

Fernandez, D. M., J. F. Vesecky, and C. C. Teague (1996), Measurements of upper ocean surface current shear with high-frequency radar, *J. Geophys. Res.*, *101*, 28,615–28,625, doi:10.1029/96JC03108.

Fleischbein, J. H., A. Huyer, P. M. Kosro, R. L. Smith, and P. A. Wheeler (2005), Upper ocean water properties and currents along paired sections in the Northern California Current, summer 1998–2003, *Data Rep. 201*, Coll. of Oceanic and Atmos. Sci., Oreg. State Univ., Corvallis, Oreg.

Geier, S. L., B. M. Hickey, S. R. Ramp, P. M. Kosro, N. B. Kachel, and F. Bahr (2006), Interannual variability in water properties and velocity in the U. S. Pacific Northwest coastal zone, *EOS Trans. AGU*, *87*(36), Ocean Sci. Meet. Suppl., Abstract OS36D–23.

Harms, S., and C. Winant (1994), Synthetic subsurface pressure derived from bottom pressure and tide gauge observations, *J. Atmos. Oceanic Technol.*, *11*, 1625–1637, doi:10.1175/1520-0426(1994)011<1625:SSPDFB>2.0.CO;2.

Hickey, B. M. (1979), The California Current System—Hypotheses and facts, *Prog. Oceanogr.*, *8*, 191–279, doi:10.1016/0079-6611(79)90002-8.

Hickey, B. M. (1998), Coastal oceanography of western North America from the tip of Baja California to Vancouver Island, in *The Sea*, edited by A. R. Robinson and K. H. Brink, pp. 345–393, John Wiley, New York.

Hickey, B. M., A. MacFadyen, W. Cochlan, R. Kudela, K. Bruland, and C. Trick (2006), Evolution of chemical, biological, and physical water properties in the northern California Current in 2005: Remote or local wind forcing?, *Geophys. Res. Lett.*, *33*, L22S02, doi:10.1029/2006GL026782.

Huyer, A. (1977), Seasonal variation in temperature, salinity, and density over the continental shelf off Oregon, *Limnol. Oceanogr.*, *22*(3), 442–453.

Huyer, A., R. L. Smith, and E. J. C. Sobey (1978), Seasonal differences in low-frequency currents fluctuations over the Oregon continental shelf, *J. Geophys. Res.*, *83*, 5077–5089, doi:10.1029/JC083iC10p05077.

Huyer, A., E. J. C. Sobey, and R. L. Smith (1979), The spring transition in currents over the Oregon continental shelf, *J. Geophys. Res.*, *84*, 6995–7011, doi:10.1029/JC084iC11p06995.

Huyer, A., J. H. Fleischbein, J. Keister, P. M. Kosro, N. Perlin, R. L. Smith, and P. A. Wheeler (2005), Two coastal upwelling domains in the northern California Current system, *J. Mar. Res.*, *63*, 901–929, doi:10.1357/002224005774464238.

Huyer, A., P. A. Wheeler, P. T. Strub, R. L. Smith, R. Letelier, and P. M. Kosro (2007), The Newport Line off Oregon—Studies in the Northeast Pacific, *Prog. Oceanogr.*, *75*, 126–160, doi:10.1016/j.pocean.2007.08.003.

Johnson, E. S., F. Bonjean, G. S. E. Lagerloef, J. T. Gunn, and G. T. Mitchum (2007), Validation and error analysis of OSCAR sea surface

currents, *J. Atmos. Oceanic Technol.*, *24*, 688–701, doi:10.1175/JTECH1971.1.

Kelly, K. A., R. C. Beardsley, R. Limeburner, K. H. Brink, J. D. Paduan, and T. K. Chereskin (1998), Variability of the near-surface eddy kinetic energy in the California Current based on altimetric, drifter, and moored current data, *J. Geophys. Res.*, *103*, 13,067–13,084, doi:10.1029/97JC03760.

Kosro, P. M. (2003), Enhanced southward flow over the Oregon shelf in 2002: A conduit for subarctic water, *Geophys. Res. Lett.*, *30*(15), 8023, doi:10.1029/2003GL017436.

Kosro, P. M. (2005), On the spatial structure of coastal circulation off Newport, Oregon, during spring and summer 2001, in a region of varying shelf width, *J. Geophys. Res.*, *110*, C10S06, doi:10.1029/2004JC002769.

Kosro, P. M. (2006), Charting the time-varying surface circulation off Oregon, *Eos Trans. AGU*, *87*(36), Ocean Sci. Meet. Suppl., Abstract OS23B–05.

Kundu, P. K., and J. S. Allen (1976), Some three dimensional characteristics of low-frequency current fluctuations near the Oregon coast, *J. Phys. Oceanogr.*, *6*, 181–199, doi:10.1175/1520-0485(1976)006<0181:STDCOL>2.0.CO;2.

Kundu, P. K., J. S. Allen, and R. L. Smith (1975), Modal decomposition of the velocity field near the coast of Oregon, *J. Phys. Oceanogr.*, *5*, 683–704, doi:10.1175/1520-0485(1975)005<0683:MDOTVF>2.0.CO;2.

Lambin, J., A. Lombard, and N. Picot (2008), CNES initiative for altimeter processing in coastal zone: PISTACH, paper presented at the First Coastal Altimeter Workshop, Centre Natl. D'Etud. Spatiales, Silver Spring, Md., 5–7 Feb.

Le Traon, P. Y., and G. Dibarboure (2002), Velocity mapping capabilities of present and future altimeter missions: The role of high frequency signals, *J. Atmos. Oceanic Technol.*, *19*, 2077–2088, doi:10.1175/1520-0426(2002)019<2077:VMCOPA>2.0.CO;2.

Le Traon, P. Y., and F. Ogor (1998), ERS-1/2 orbit improvement using Topex/POSEIDON: The 2 cm challenge, *J. Geophys. Res.*, *103*, 8045–8058, doi:10.1029/97JC01917.

Le Traon, P. Y., Y. Faugère, F. Hernandez, J. Dorandeu, F. Mertz, and M. Ablain (2003), Can we merge GEOSAT follow-on with Topex/Poseidon and ERS-2 for an improved description of the ocean circulation?, *J. Atmos. Oceanic Technol.*, *20*, 889–895, doi:10.1175/1520-0426(2003)020<0889:CWMGFW>2.0.CO;2.

Leeuwenburgh, O., and D. Stammer (2002), Uncertainties in altimetry-based velocity estimates, *J. Geophys. Res.*, *107*(C10), 3175, doi:10.1029/2001JC000937.

Lentz, S. (1993), The accuracy of tide-gauge measurements at subtidal frequencies, *J. Atmos. Oceanic Technol.*, *10*, 238–245, doi:10.1175/1520-0426(1993)010<0238:TAOTGM>2.0.CO;2.

Leuliette, E. W., R. S. Nerem, and G. T. Mitchum (2004), Calibration of Topex/Poseidon and Jason altimeter data to construct a continuous record of mean sea level change, *Mar. Geod.*, *27*, 79–94, doi:10.1080/01490410490465193.

Lillibridge, J. (2005), Coastal altimetry challenges, paper presented at Science Review Meeting, Coop. Inst. for Oceanogr. Satell. Stud., Corvallis, Oreg.

Lipa, B. J., and D. E. Barrick (1983), Least-squares methods for the extraction of surface currents from CODRA crossed-loop data: Application at ARSLOE, *IEEE J. Oceanic Eng.*, *8*, 226–253, doi:10.1109/JOE.1983.1145578.

Mackas, D. L., P. T. Strub, A. C. Thomas, and V. Montecino (2006), Eastern ocean boundaries—Pan regional overview, in *The Sea: The Global Coastal Ocean, Interdisciplinary Regional Studies and Syntheses: Pan-Regional Syntheses and the Coasts of North and South America and Asia*, edited by A. R. Robinson and K. H. Brink, pp. 21–60, Harvard Univ. Press, Cambridge, Mass.

Madsen, K. S., J. L. Høyer, and C. C. Tscherning (2007), Near-coastal satellite altimetry: Sea surface height variability in the North Sea–Baltic Sea area, *Geophys. Res. Lett.*, *34*, L14601, doi:10.1029/2007GL029965.

Manzella, G. M. R., G. Borzelli, P. Cipollini, T. H. Guymer, H. M. Snaith, and S. Vignudelli (1997), Potential use of satellite data to infer the circulation dynamics in a marginal area of the Mediterranean Sea, *Rep. ESA SP-414*, Eur. Space Agency, Noordwijk, Netherlands.

Marcotte, D. (1991), Cokriging with MATLAB, *Comput. Geosci.*, *17*(9), 1265–1280, doi:10.1016/0098-3004(91)90028-C.

Pascual, A., Y. Faugere, G. Larnicol, and P.-Y. Le Traon (2006), Improved description of the ocean mesoscale variability by combining four satellite altimeters, *Geophys. Res. Lett.*, *33*, L02611, doi:10.1029/2005GL024633.

Pascual, A., M. I. Pujol, G. Larnicol, P. Y. Le Traon, and M. H. Rio (2007), Mesoscale mapping capabilities of multisatellite altimeter missions: First results with real data in the Mediterranean, *J. Mar. Syst.*, *65*(1–4), 190–211, doi:10.1016/j.jmarsys.2004.12.004.

Smith, R. L. (1978), Poleward propagating perturbations in currents and sea level along the Peru coast, *J. Geophys. Res.*, *83*, 6083–6092, doi:10.1029/JC083iC12p06083.

Smith, W. H. F., P. T. Strub, and L. Miller (2008), First coastal altimetry workshop held, *Eos Trans. AGU*, *89*(40), doi:10.1029/2008EO400008.

Stewart, R. H., and J. W. Joy (1974), HF radio measurements of surface currents, *Deep Sea Res. Oceanogr. Abstr.*, *21*, 1039–1049.

Strub, P. T., and C. James (1997), Satellite comparisons of Eastern Boundary Currents: Resolution of circulation features in "coastal" oceans, paper presented at Monitoring the Oceans in the 2000s: An Integrated Approach, Centre Natl. d'Etud. Spatiale, Biarritz, France.

Strub, P. T., and C. James (2000), Altimeter-derived variability of surface velocities in the California Current System: 2. Seasonal circulation and eddy statistics, *Deep Sea Res., Part II*, *47*, 831–870, doi:10.1016/S0967-0645(99)00129-0.

Strub, P. T., and C. James (2002a), Altimeter-derived surface circulation in the large-scale NE Pacific gyres — Part 1. Seasonal variability, *Prog. Oceanogr.*, *53*, 163–183, doi:10.1016/S0079-6611(02)00029-0.

Strub, P. T., and C. James (2002b), The 1997–1998 oceanic El Nino signal along the southeast and northeast Pacific boundaries—An altimetric view, *Prog. Oceanogr.*, *54*, 439–458, doi:10.1016/S0079-6611(02)00063-0.

Strub, P. T., J. S. Allen, A. Huyer, and R. C. Beardsley (1987), Seasonal cycles of currents, temperatures, winds, and sea level over the Northeast Pacific Continental Shelf: 35°N to 48°N, *J. Geophys. Res.*, *92*, 1507–1526, doi:10.1029/JC092iC02p01507.

Sudre, J., and R. A. Morrow (2008), Global surface currents: A high-resolution product for investigating ocean dynamics, *Ocean Dyn.*, *58*, 101–118, doi:10.1007/s10236-008-0134-9.

Vignudelli, S., P. Cipollini, M. Astraldi, G. P. Gasparini, and G. Manzella (2000), Integrated use of altimeter and in situ data for understanding the water exchanges between the Tyrrhenian and Ligurian seas, *J. Geophys. Res.*, *105*, 19,649–19,664, doi:10.1029/2000JC900083.

Vignudelli, S., P. Cipollini, L. Roblou, F. Lyard, G. P. Gasparini, G. Manzella, and M. Astraldi (2005), Improved satellite altimetry in coastal systems: Case study of the Corsica Channel (Mediterranean Sea), *Geophys. Res. Lett.*, *32*, L07608, doi:10.1029/2005GL022602.

Vignudelli, S., P. Berry, and L. Roblou (2008), Satellite altimetry near coasts—Current practices and a look at the future, paper presented at 15 Years of Progress in Radar Altimetry, Eur. Space Agency, Venice, Italy, 6 Oct.

Volkov, D. L., G. Larnicol, and J. Dorandeu (2007), Improving the quality of satellite altimetry data over continental shelves, *J. Geophys. Res.*, *112*, C06020, doi:10.1029/2006JC003765.

P. M. Kosro and P. T. Strub, College of Oceanic and Atmospheric Sciences, Oregon State University, 104 COAS Administration Building, Corvallis, OR 97331-5503, USA.

M. Saraceno, Centro de Investigaciones del Mar y la Atmosfera, Ciudad Universitaria, Intendente Guiraldes 2160, Pab. II, 2do piso, Ciudad de Buenos Aires, C1428EGA, Argentina. (saraceno@cima.fcen.uba.ar)